



# Annexin A1-FPR1 Interaction in dendritic cells promotes immune microenvironment modulation in Thyroid Cancer

Hongwei Jiang · Lirun Kuang · Tianyi Zhang · Xupeng Zhao

Received: 10 January 2025 / Accepted: 9 May 2025  
© The Author(s) 2025

**Abstract** Thyroid cancer (THCA) is profoundly influenced by its immune microenvironment, with dendritic cells (DCs) serving as key mediators of tumor-immune interactions. This study leveraged single-cell RNA sequencing and transcriptome RNA sequencing to analyze DC populations in THCA tissues. The results revealed significant disparities in DC distribution and function, with formyl peptide receptor 1 (FPR1) emerging as a crucial factor associated with patient prognosis. Meta-analysis further validated the differential expression of FPR1, reinforcing its significance in THCA progression. Investigations into the TME highlighted the relationship between FPR1 and DC maturation and activation, elucidating the mechanistic basis for immune regulation. Experimental validation confirmed that Annexin A1 (ANXA1) interacts with FPR1 in DCs, promoting tumor progression through immune modulation. These findings advance the understanding of THCA

immune mechanisms and underscore the potential of targeting the ANXA1-FPR1 axis as a novel approach for immunotherapy in THCA.

**Keywords** Thyroid Cancer · Tumor Microenvironment · Dendritic Cells · Formyl Peptide Receptor 1 · Annexin A1 · Immunotherapy Strategies

## Introduction

The rapid advancement of modern medical technology highlights the tumor microenvironment (TME) as a pivotal determinant of tumor behavior and treatment outcomes (Tong et al. 2022; Hinshaw and Shevde 2019; Pansy et al. 2021). Composed of malignant cells, infiltrating immune cells, fibroblasts, and vascular cells, the TME form a dynamic signaling milieu rich in cytokines, chemokines, and growth factors (Feng et al. 2022; Tauriello et al. 2021; Portella et al. 2021). Within this microenvironment, immune cells, particularly dendritic cells (DCs), play a vital role by facilitating antigen presentation to and activation of T cells, thereby initiating an immune response against tumors (Ronca et al. 2020; Fu and Jiang 2018; Garris and Luke 2020; Wang et al. 2020a, b, c).

Thyroid cancer (THCA), as a prevalent endocrine malignancy, continues to show an increasing incidence globally (Cao et al. 2021; Prete et al. 2020; Franchini et al. 2022). Although most THCA patients have a favorable prognosis following surgery

---

<sup>§</sup>Hongwei Jiang, Lirun Kuang, and Tianyi Zhang contributed equally to this work.

---

**Supplementary Information** The online version contains supplementary material available at <https://doi.org/10.1007/s10565-025-10042-6>.

---

H. Jiang · L. Kuang · T. Zhang · X. Zhao (✉)  
Department of General Surgery, the Fourth Affiliated Hospital of China Medical University, No. 4, Chongshan Dong Road, Huanggu District, Shenyang 110032, P. R. China  
e-mail: zhaoxp\_0@163.com

and radioactive iodine therapy, some still experience recurrence and distant metastasis (Kakudo et al. 2021; Ulisse et al. 2021; Fallahi et al. 2022; Chou et al. 2022). Recent advances in immunotherapy, particularly the use of immune checkpoint inhibitors (ICIs), has demonstrated potential efficacy for high-risk patients (Sellars et al. 2022; Muir et al. 2022). Therefore, investigating the key signaling pathways within the THCA TME and their interactions with immune cells holds significance in improving therapeutic strategies for THCA.

Annexin A1 (ANXA1) and formyl peptide receptor 1 (FPR1) have recently attracted considerable attention for their roles across multiple tumor types. ANXA1, a protein with diverse biological functions, regulates inflammatory responses and influences tumor cell migration, invasion, and immune cell functionality through its interaction with FPR1, playing a crucial role in tumor immune regulation (Zhao et al. 2022; Foo et al. 2019; Araújo et al. 2021). Notably, ANXA1 has been found to promote tumor cell growth and dissemination in some studies, with FPR1 being its primary functional receptor, indicating their significant roles in tumor initiation, progression, and immune response regulation (Feng et al. 2020; Wu et al. 2022). Within the TME, ANXA1 activates relevant signaling pathways through FPR1, enabling tumor cells to evade immune surveillance and enhance their survival and proliferation. Moreover, ANXA1 can reprogram the immune landscape of TME by influencing DC and T cell functionality (Feng et al. 2020). However, the specific mechanisms of action of ANXA1 and FPR1 in THCA, a distinct tumor type, remain incompletely understood. While some research indicates a correlation between ANXA1 expression in THCA cells and malignancy, there is still insufficient understanding of how these molecules specifically regulate the immune microenvironment of THCA and how they promote progression through immune pathways (Zhang et al. 2022). Therefore, recent documents have also explored the significance of ANXA1 in THCA, particularly its regulation of the immune microenvironment. Liu et al. (2025) found that exosomal ANXA1 promotes immune evasion in papillary thyroid carcinoma (PTC) by influencing macrophage M2 polarization (Liu 2024). Additionally, Chen et al. (2022a, b) revealed changes in immune cell gene expression through single-cell RNA sequencing (scRNA-seq),

and found that ANXA1 was closely linked to alterations in the immune microenvironment of PTC and patient prognosis (Chen et al. 2022a, b). These findings further validate the regulatory role of ANXA1 in the immune microenvironment of THCA, enhancing our understanding of its role in immune modulation in THCA. Therefore, dissecting ANXA1-FPR1 interactions in THCA could uncover their significance in THCA progression and inform innovative treatment modalities.

Against this backdrop, this study employs scRNA-seq and transcriptome RNA sequencing data to offer a unique perspective on the mechanisms of DCs within the THCA TME. The scRNA-seq technology reveals the heterogeneity and complex cell states within cell populations, which is crucial for understanding how DCs modulate the immune response in THCA. Furthermore, by integrating transcriptome data from public databases like The Cancer Genome Atlas (TCGA) and Gene Expression Omnibus (GEO), this study not only evaluates the expression differences in DC marker genes but also delves into their prognostic value. The study aims to delve deep into how the ANXA1-FPR1 signaling pathway in the THCA TME influences the maturation and activation of DCs, thereby participating in the occurrence and progression of THCA. This study probes into novel targets and strategies for precise THCA therapy, with the goal of enhancing patient outcomes and quality of life, thus holding significant scientific and clinical implications.

## Materials and methods

### Downloading transcriptome sequencing data

The scRNA-seq dataset GSE184362, comprising tumor and adjacent normal tissues from 13 THCA patients, was retrieved from the GEO database (<http://www.ncbi.nlm.nih.gov/geo/>). Additional GEO-derived transcriptome datasets used for meta-analysis are summarized in Table S1.

Bulk RNA-seq data (HTSeq-FPKM) for 512 THCA and 59 normal thyroid samples, together with clinical annotations, were accessed from the TCGA-THCA project (<https://portal.gdc.cancer.gov/>). To supplement the number of normal tissues, RNA expression profiles from 278 healthy thyroid samples

were obtained via the GTEx portal (<https://www.gtexportal.org/home/index.html>). Since all datasets were publicly available, no additional ethical approval was necessary (Zhao et al. 2020).

#### scRNA-Seq data processing

Gene expression matrices were generated using Cell Ranger (10 × Genomics). Cells were filtered in light of the following thresholds: nFeature\_RNA between 200 and 5000, nCount\_RNA between 1000 and 20,000, and mitochondrial gene content (percent.mt) below 15%. Data quality was tested via unique molecular identifier (UMI) counts and gene correlation analyses. Principal component analysis (PCA) was done on highly variable genes utilizing the Seurat R package (Hao et al. 2021) for dimensionality reduction. The clustering resolution was determined based on the top 10 principal components (PCs) identified in PCA using the UMAP algorithm. The chosen clustering resolution effectively distinguished major cell types without over-partitioning, resulting in 18 initial clusters. The above-mentioned clusters were further annotated into seven different cell types based on known cell marker genes. The JackStraw and Elbow-Plot functions guided PC selection, after which clustering was done utilizing a graph-based method and visualized via UMAP. Cell types were annotated in light of established marker genes (Meng et al. 2021). Pseudotime trajectory analysis was done with the help of Monocle2 (v2.22.0; (Qiu et al. 2017)).

#### Cellular communication analysis in the TME

The CellChat tool (v1.1.3, (Fang et al. 2022)) was used to analyze cellular communication patterns within the TME. First, the normalized gene expression data were input into CellChat for preprocessing, including steps such as identifyOverExpressedGenes, identifyOverExpressedInteractions, and projectData, to ensure result robustness. Next, the aggregateNet and computeCommunProb functions were used to calculate the communication probability and information flow intensity of ligand-receptor (L-R) pairs between cell populations, constructing a cellular communication network in the TME. To further explore key ligand-receptor-related genes, the CellPhoneDB tool (v2.1.4, (Efremova et al. 2020)) was also used. The normalized gene expression matrix was input,

and preprocessing was performed to identify receptor-ligand pairs between cells. By calculating the significance ( $P < 0.05$ ) and interaction strength of receptor-ligand molecular pairs, 41 ligand-receptor genes closely related to TME regulation and treatment response were screened, providing a basis for further mechanistic research.

#### Gene function enrichment analysis

DC-specific marker genes ( $n = 833$ ) were subjected to Gene Ontology (GO) and Kyoto Encyclopedia of Genes and Genomes (KEGG) enrichment analyses using the clusterProfiler R package, with significance set at  $P < 0.05$ . GO terms were classified into biological processes (BP), cellular components (CC), and molecular functions (MF) (Yu et al. 2012).

#### Single gene survival analysis

The prognostic relevance of SPP1, IL1B, CD74, IFNGR1, CXCL16, TNFSF13B, AXL, FPR1, IFNGR2, LGALS9, HAVCR2, CD4, TNF, CXCR3, GAS6, CXCR4, and ANXA1 in THCA was assessed utilizing clinical data from the TCGA-THCA cohort. Overall survival (OS) was selected as the endpoint. Cox proportional hazards models were made with the help of the R package *survival*, and survival curves were generated employing *survminer* and *ggplot2*. Group differences in OS between high- and low-expression cohorts were evaluated by the Log-rank test, with  $P < 0.05$  deemed statistical significance (Zhao et al. 2021).

#### Correlation analysis

Based on the TCGA-THCA dataset, the expression correlation between FPR1 and ANXA1 in tumor tissues was examined employing the R package *corrplot*. Additionally, correlations between FPR1 and 47 immune checkpoint-related genes (e.g., IDO1, IDO2, LAG3, CTLA4, TNFRSF9, ICOS, CD80, PDCD1LG2, TIGIT, CD70, TNFSF9, ICOSLG, KIR3DL1, CD86, PDCD1, LAIR1, TNFRSF8, TNFSF15, TNFRSF14, CD276, CD40, TNFRSF4, TNFSF14, HHLA2, CD244, CD274, HAVCR2, CD27, BTLA, LGALS9, TMIGD2, CD28, CD48, TNFRSF25, CD40LG, ADORA2 A, VTCN1, CD160, CD44, TNFSF18, TNFRSF18, BTNL2,

C10orf54, CD200R1, TNFSF4, CD200, and NRP1 were analyzed (Xu et al. 2022).

#### Analysis of differential gene expression

The TCGA-THCA dataset and GTEx dataset were utilized to test the differential expression of FPR1 and ANXA1 in THCA tissues. The analysis was completed utilizing the R software package limma, with a threshold set at  $\log_2\text{FC} > 1$  and  $P < 0.05$  (Ritchie et al. 2015).

#### Meta-analysis

Meta-analysis was done utilizing the R package *meta*, with the standard mean difference (SMD) and 95% confidence interval (CI) as effect size measures. Heterogeneity across studies was evaluated employing the Q-test and chi-square test, with  $I^2$  and  $P$  values guiding model selection: a fixed-effects model was made when  $P > 0.05$  and  $I^2 < 50\%$ , indicating low heterogeneity, otherwise a random-effects model was utilized.

Subgroup analyses were conducted based on detection methods (RNA-seq vs. microarray). Sensitivity analysis was done utilizing a leave-one-out approach, sequentially excluding each study to assess the robustness of the pooled effect and to identify studies significantly impacting the association between FPR1, ANXA1, and THCA outcomes (Balduzzi et al. 2019).

#### TME analysis

The TME was tested utilizing the R package *estimate* by calculating the StromalScore, ImmuneScore, and ESTIMATEScore for each sample. Differences in these scores between high- and low-expression groups of FPR1 and ANXA1 were subsequently compared (Huang et al. 2020).

#### Analysis of immune cell infiltration

The enrichment scores of 24 immune cell-related functional marker genes were calculated using the R software package GSEA for single sample gene set enrichment analysis (ssGSEA) based on a study by Bindea et al. (Hänzelmann et al. 2013). The markers for the 24 immune cells provided in the Immunity

article by Bindea et al. were employed to assess the immune infiltration status in TCGA-THCA data (Bindea et al. 2013).

#### Analysis of immunotherapy in THCA patients

Immunotherapy data for THCA patients were gained from the TCIA database (<https://tcia.at/>). The Immunophenoscore (IPS) was utilized to predict responses to cytotoxic T-lymphocyte antigen 4 (CTLA-4) and programmed cell death protein 1 (PD-1) blockade. Differences in IPS between high- and low-expression groups of FPR1 were checked utilizing the R package *ggpubr* (Zanfardino et al. 2019).

#### Cell culture

Human PTC cell line TPC-1 (CL-0643, Procell), B-CPAP (CL-0575, Procell), human peripheral blood DCs (CP-H179B, Procell), and human peripheral blood CD3<sup>+</sup> T cells (PRI-H-00107, Xqxbio) were cultured in RPMI 1640 (72,400,120, Gibco) containing 10% FBS (10,437,010, Gibco) and 1% penicillin–streptomycin (15,140,163, Gibco). The cultures were maintained at 37 °C in a 5% CO<sub>2</sub> atmosphere. When cell confluence reached 60–80%, passaging and transfection were performed (Chen et al. 2022a, b) (Chen et al. 2022a, b).

#### Immunoprecipitation

DCs were lysed in RIPA buffer (P0013 C, Beyotime, Shanghai, China), and cellular debris was removed by centrifugation. The supernatant was harvested, and the supernatant of each sample was adjusted to the same concentration. Input controls were reserved; the resultant supernatant was immunoprecipitated with anti-ANXA1 (ab214486, Abcam, 1:2000, UK) or anti-FPR1 antibody (ab113531, Abcam, 1:500, UK) along with protein A/G beads (Santa Cruz Biotechnology) for 2 h. Subsequently, beads were triple-washed, denatured at 100 °C for 5 min, electrophoresed, transferred to nitrocellulose membranes (Millipore, Temecula, CA, USA), and subjected to immunoblotting (Chen et al. 2023).

## Preparation of lentiviral vectors

The lentiviral vector pSIH1-H1-copGFP (sh-; SI501 A-1, System Biosciences, USA) was adopted for ANXA1 knockdown, while pCDH-CMV-MCS-EF1 $\alpha$ -copGFP (oe-; CD511B-1) facilitated FPR1 overexpression. Lentiviral particles were generated by transfecting HEK-293 T cells (iCell-h237, Cell Applications, Shanghai, China) with a packaging kit (A35684 CN, Invitrogen, USA). After 48 h, viral supernatants ( $1 \times 10^8$  TU/mL) were harvested. Target cells at ~40% confluence were transduced with the viral suspension for 8 h, followed by culture in DMEM enriched with 10% fetal bovine serum (FBS). Puromycin (5  $\mu$ g/mL; A1113803, Thermo Fisher Scientific, China) selection was applied for 4 weeks. Table 1 summarizes lentiviral sequences. Silencing efficiency was verified in DC cells (Figure S1), and the most effective sequence (sh-ANXA1-1) was utilized in subsequent experiments (Vecchi et al. 2018).

## Cell Co-culture system

To assess the stimulatory capacity of DC, the transfected DCs from each group were co-cultured with CD3 + T cells at a ratio of 1:10 (DCs: T) in a 96-well plate:  $3 \times 10^5$  DCs from each group were added along with  $3 \times 10^6$  CD3 + T cells, and the culture volume was adjusted to 200  $\mu$ L with RPMI 1640 medium. The cells were then incubated at 37 °C with 5% CO<sub>2</sub>. After 72 h of cultivation, CD3<sup>+</sup> T cell proliferation was tested utilizing the CCK-8 assay. For the evaluation of DCs' phagocytic ability,  $1 \times 10^5$  cells from each group were suspended in 200  $\mu$ L RPMI 1640 medium and incubated with FITC-Dextran (100  $\mu$ g/mL; D1844, Invitrogen™) for 4 h. FITC uptake was quantified via flow cytometry.

To investigate the impact of DC cells on TPC-1 cells, 100  $\mu$ L (containing  $1 \times 10^4$  cells) of TPC-1 cells were supplemented to each well of a 96-well plate. Subsequently, CD3 + T cells from the co-culture with respective DC groups were added at a ratio of 1:10 (T: TPC-1) to the TPC-1 cells, and the final volume was adjusted to 200  $\mu$ L. The co-culture was maintained in a 37 °C, 5% CO<sub>2</sub> culture system for 48 h, after which TPC-1 cells were harvested for further analysis (Fang et al. 2021).

## Transwell assay

TPC-1 cells were evaluated for migratory and invasive capacities employing 24-well Transwell chambers (8  $\mu$ m pore size; #3422, Corning, NY, USA). For invasion assays, chambers were pre-coated with Matrigel (#354,277, BD Biosciences, CA, USA), diluted 1:1 with serum-free medium and solidified at 37 °C. Migration assays omitted Matrigel pretreatment.

Cells ( $2 \times 10^5$ ) suspended in 200  $\mu$ L serum-free medium were loaded into the upper chambers; 800  $\mu$ L of 20% FBS medium was placed in the lower wells. After 24 h at 37 °C, membranes were processed by PBS washing, fixation with 4% paraformaldehyde, 0.1% crystal violet staining, imaged in five random fields (Nikon Eclipse Ci, Nikon, Tokyo, Japan), and quantified over three replicates (Hou et al. 2021).

## Clonogenic assay

A clonogenic assay was utilized to check the TPC-1 cell proliferative capacity. Cells were inoculated at a density of 2000 cells per 6 cm culture dish. After changing the culture medium, the cells were allowed to grow for 14 days. Subsequently, staining was performed using 0.5% (w/v) crystal violet (C8470, Solebao Technologies, Beijing, China), followed by imaging and quantification of colony formation. Clusters of cells consisting of more than 50 cells were identified as a single clone (Wang et al. 2020a, b, c).

## CCK-8 assay

Logarithmically growing cells were seeded at  $5 \times 10^4$  cells/well in 96-well plates for overnight culturing. Cell viability was examined utilizing the CCK-8 kit (E606335, Sangon Biotech, China) by adding 10  $\mu$ L of reagent at 0, 24, 48, and 72 h. Following 1 h of incubation at 37 °C in 5% CO<sub>2</sub>, absorbance at 450 nm was documented with an Epoch microplate reader (BioTek, USA) (Guo et al. 2019; Wang et al. 2020a, b, c; Luo et al. 2018). Each condition was tested in triplicate across three independent experimentations.

## Ethical statement

All animal experiments were conducted under protocols approved by the institutional Animal Ethics

Committee, in compliance with established guidelines. Every effort has been made to minimize the pain and distress experienced by the animals, as well as to reduce the number of animals required for experimentation. Animal housing, care, and experimentations were done in light of internationally accepted standards for animal welfare. Adequate care has been provided to all animals, and measures have been taken to ensure their proper disposition after the conclusion of the experiments.

#### Construction of subcutaneous tumor model in Mice

Eighteen 6-week-old male NCG nude mice weighing  $20 \pm 2$  g were procured from Jicuiyaokang. They were housed in SPF conditions with a 12-h light–dark cycle, and a suitable temperature range of 22–25 °C. Prior to cell injection, DCs and T cells, along with TPC-1 cells, were transfected in a 200  $\mu$ L system containing a ratio of  $5 \times 10^5$  DCs,  $5 \times 10^5$  T cells, and  $1 \times 10^6$  TPC-1 cells. Subsequently, the mice were randomized into the sh-NC + oe-NC, sh-ANXA1 + oe-NC, and sh-ANXA1 + oe-FPR1 groups, with each group receiving a subcutaneous injection of 200  $\mu$ L of the corresponding cell mixture into the left abdominal wall. Tumor volume was tested every two days. On the 12 th day post-injection, the studied animals were anesthetized with 50 mg/kg pentobarbital sodium (B005, Jiancheng, Nanjing, China), then euthanized by cervical dislocation at the point of neck dislocation, followed by tumor removal, photography, weighing, and storage for subsequent detection of relevant factor expression. To minimize subjective bias, three independent researchers assessed each sample separately (Luo et al. 2023).

#### RT-qPCR

Tissues were processed for RNA extraction utilizing Trizol (16,096,020, Invitrogen, USA). cDNA was synthesized via RT with the Takara kit (RR047 A, Japan). Gene expression analysis was done via RT-qPCR utilizing TaqMan assays (Applied Biosystems, Foster City, CA, USA), with GAPDH as the endogenous control. Each RT-qPCR experiment was conducted in triplicate wells. Primer sequences are detailed in Table 2. The fold change in target gene expression patterns was computed utilizing the  $2^{-\Delta\Delta Ct}$  method (Wang et al. 2023).

#### Western Blot

Following protein extraction utilizing RIPA buffer, its concentration was checked via BCA assay (20201ES76, Yisheng Biotechnology, Shanghai) and normalized. SDS-PAGE was used for protein separation, followed by transfer to PVDF membranes (IPVH85R, Millipore, Germany) via wet transfer. Membranes were blocked with 5% BSA at ambient temperature for 1 h, followed by overnight incubation at 4 °C with anti-ANXA1 (ab214486, Abcam, UK), anti-FPR1 (PA1-41,398, Invitrogen, USA), anti-BATF3 (ab211304, Abcam, UK), and anti-GAPDH (ab9485, Abcam, UK). After TBST washes, secondary antibody incubation was done with HRP-conjugated goat anti-rabbit IgG (ab6721, Abcam, UK) for 1 h. Chemiluminescent signals were developed and analyzed with ImageJ (NIH) to calculate relative protein expression using GAPDH as the control (Wang et al. 2023). For the full length uncropped original western blots, please refer to Supplemental Material file.

#### Immunofluorescence staining

After formalin fixation and paraffin embedding, tissue sections underwent deparaffinization, antigen retrieval (10 mM sodium citrate, pH 6.0), and blocking with 10% goat serum. Primary antibodies—anti-ANXA1 (ab214486, Abcam, UK), anti-FPR1 (ab113531, Abcam, UK), and anti-BATF3 (ab302568, Abcam, UK)—were applied overnight at 4 °C. After washing, secondary antibodies (fluorescent anti-rabbit IgG, ab150079, Abcam, UK) were incubated at ambient temperature for 1 h, in the dark. Nuclei were counterstained with DAPI (D1306, ThermoFisher, USA) for 10 min. After final washes, slides were mounted with anti-fade medium and imaged utilizing a fluorescence microscope. Quantification of positive cells was done employing ImageJ or built-in software (Zheng et al. 2022).

#### Flow cytometry

Tumor tissue was digested in HBSS (with Ca/Mg) enriched with DNase I (10  $\mu$ g/mL) and Liberase (25  $\mu$ g/mL) at 37 °C for 30 min with intermittent shaking. The suspension was filtered via a 70  $\mu$ m mesh, cold PBS-rinsed, and centrifuged at 1000  $\times$ g for 5 min

at 4 °C. Red blood cells were lysed utilizing ACK buffer (A1049201, Invitrogen), quenched with PBS, and centrifuged again. Cell pellets were resuspended in FACS buffer for downstream analysis. For in vitro-cultured cells, after PBS washing and centrifugation under the same conditions, cells were similarly resuspended in FACS buffer.

The aforementioned cell samples were blocked with goat serum IgG (SL038, Solarbio) for 15 min and subsequently stained with a panel of antibodies according to the experimental requirements. For all channels, the gating of positive and negative cells was based on Fluorescence Minus One (FMO) control. Specific antibody-binding cell populations were identified and quantified by flow cytometry. The antibodies used included BATF3 (ab307471, Abcam), CD1a (ab256268, Abcam), CD86 (ab303578, Abcam), CD4 (ab277931, Abcam), and CD8 (ab237365, Abcam) as reported in (Mokuda et al. 2015).

### Statistical analysis

Data were initially summarized utilizing descriptive statistics (mean, median, standard deviation, range). For comparisons between two groups, an independent t-test was applied. A one-way ANOVA was adopted for comparisons across three or more groups, while MANOVA was employed for analyses involving multiple factors. Survival analysis was done employing Kaplan–Meier curves, and differences were examined with the Log-rank test. Pearson's correlation coefficient was adopted for continuous variable relationships. Linear and logistic regression were employed for predictive or exploratory analysis. For non-normally distributed data or unequal variances, non-parametric tests (Mann–Whitney U or Kruskal–Wallis) were applied. All analyses were completed utilizing SPSS (IBM) or R. Statistical significance was made at  $p < 0.05$ . Graphs were prepared with GraphPad Prism (GraphPad Software, Inc.).

## Results

### scRNA-Seq Identifies 7 Major Cell Types in THCA Patient Tumor and Adjacent Tissue Samples.

We retrieved the THCA-related scRNA-seq dataset GSE184362 from GEO, which includes 6 adjacent and 7 tumor tissue samples. After

filtering, 49,576 cells from adjacent tissues (P1–P6) and 54,293 cells from tumor tissues (T1–T7) were retained (Figure S2A, S2D). The correlation between nCount\_RNA and percent.mt was negligible ( $r = -0.01$ ), while nCount\_RNA was strongly correlated with nFeature\_RNA ( $r = 0.87$  and  $0.95$ ), confirming high data quality (Figure S2B, S2E). Following variability assessment, the 2,000 most variable genes were extracted to inform downstream analyses (Figure S2C, S2F).

Cell cycle scoring showed consistent distribution across all samples (Figure S3A). PCA of the top 2,000 highly variable genes revealed no batch effects among the 13 samples (Figure S3B). Jack-StrawPlot visualization of the top 50 PCs indicated that significant components, with  $p$ -values  $< 0.05$ , captured key information, with the first 10 PCs showing  $p$ -values below 0.05 (Figure S3C). The ElbowPlot identified a clear inflection point at the 10th PC (Figure S3D). Heatmap of the first 2 PCs generated by DimHeatmap function highlighted the key genes (Figure S3E, S3F). Consequently, further analyses leverage these 10 PCs for UMAP clustering.

Eighteen cell clusters were defined by UMAP-based analysis (Fig. 1A), later annotated into 7 distinct cell types based on cell marker genes: Neutrophils, DCs, T & NK cells, B cells, Thyrocytes, Fibroblasts, and Endothelial cells (Fig. 1B). The expression patterns of marker genes are visualized in Fig. 1C. Notably, cluster 14 represents Neutrophils, with marker genes S100A8, CXCL8, SOD2, and NAMPT; clusters 2 and 15 are identified as DCs, marked by genes HLA-DRA, HLA-DPB1, CST3, and HLA-DPA1; clusters 0, 5, 6, and 8 correspond to T & NK cells, characterized by genes CD3D, CD3E, CD2, and CD4; clusters 1, 12, and 17 indicate B cells, with marker genes CD79A, CD79B, IGHM, and IGHD; clusters 3, 4, 7, 11, 13, and 16 represent Thyrocytes, showcasing genes TG, EPCAM, KRT18, and KRT19; cluster 10 encompasses Fibroblasts, marked by COL1A1, COL1A2, COL3A1, and ACTA2; while cluster 9 identifies Endothelial cells, with marker genes PECAM1, CD34, CDH5, and VWF.

Conclusively, we constructed a single-cell transcriptome atlas comprising 103,869 cells from THCA patient tumor and adjacent tissue samples through scRNA-seq analysis.

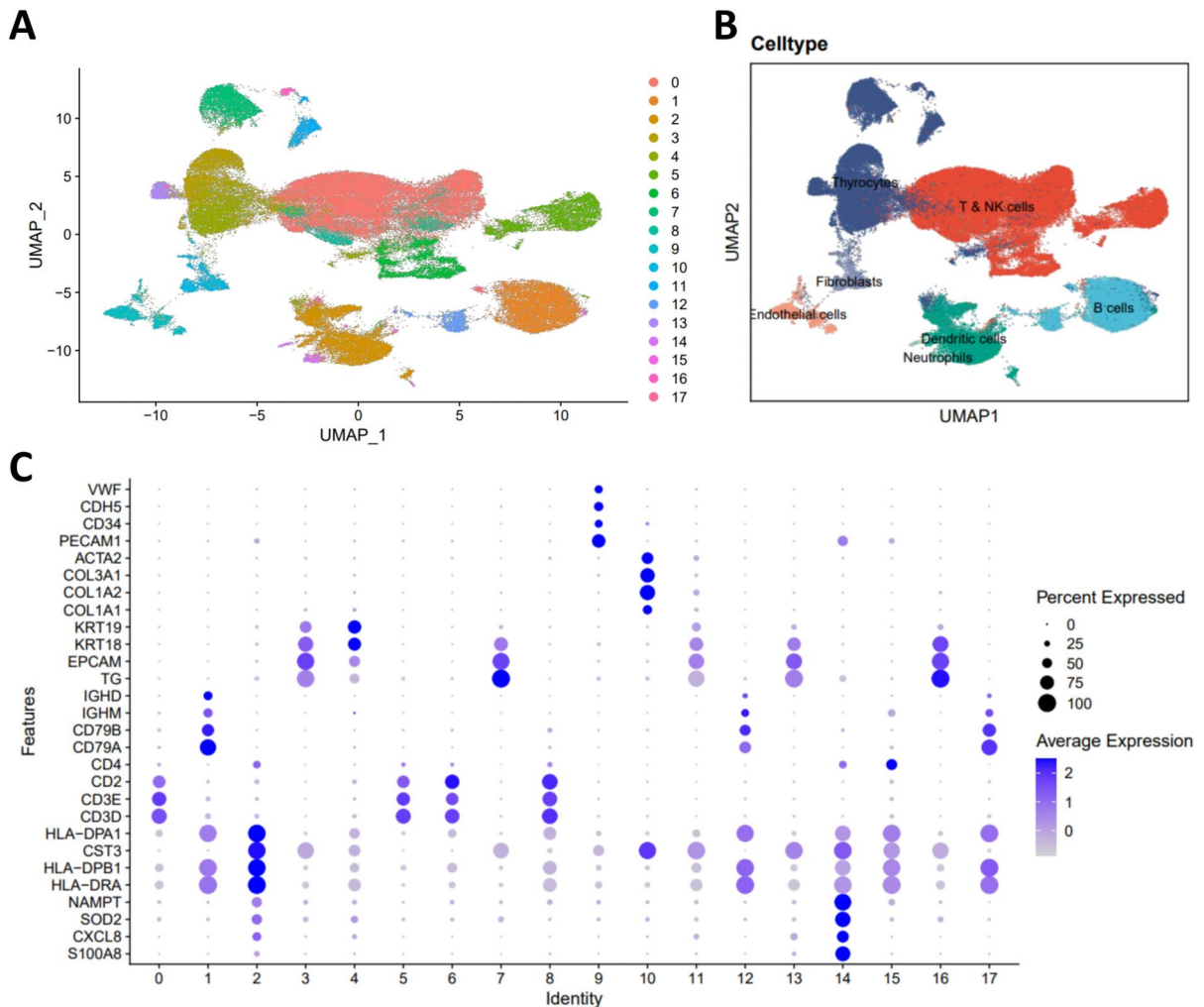


**Fig. 1** Single-Cell Transcriptomic Atlas of Cancer and Adjacent Tissues in THCA Patients. Notes: (A) UMAP analysis clustered cells into 18 cell clusters; (B) Annotation of the 18 cell clusters into 7 cell types based on expression of known

marker genes; (C) Bubble plot of expression of cell marker genes, where darker colors indicate higher expression levels and larger circles indicate higher expression proportions

### Significant changes of DCs in samples of THCA and adjacent tissues

We further compared the changes in the proportions of these seven cell types in samples of THCA and adjacent tissues. Overall, the full spectrum of seven cell types was shared across cancerous and non-malignant tissues, but their proportions varied, especially DCs (Fig. 2A). Further statistical analysis revealed a notable difference only in the proportion of DCs in samples of THCA and adjacent tissues (Fig. 2B-G).

Using an  $\text{avg\_log}_2$  FC threshold of  $>0.5$ , we extracted 833 marker genes of DCs for subsequent analysis. The results demonstrated that DC marker genes were mainly enriched in inflammatory bowel disease, Th17 cell differentiation, antigen processing and presentation, as well as signaling pathways such as Toll-like receptors, NF-kappa B, and chemokines (Fig. 3A). Additionally, DC marker genes were predominantly enriched in BP such as leukocyte cell–cell adhesion, positive regulation of cytokine production, regulation of leukocyte cell–cell adhesion, and cell activation involved in immune responses. In terms of

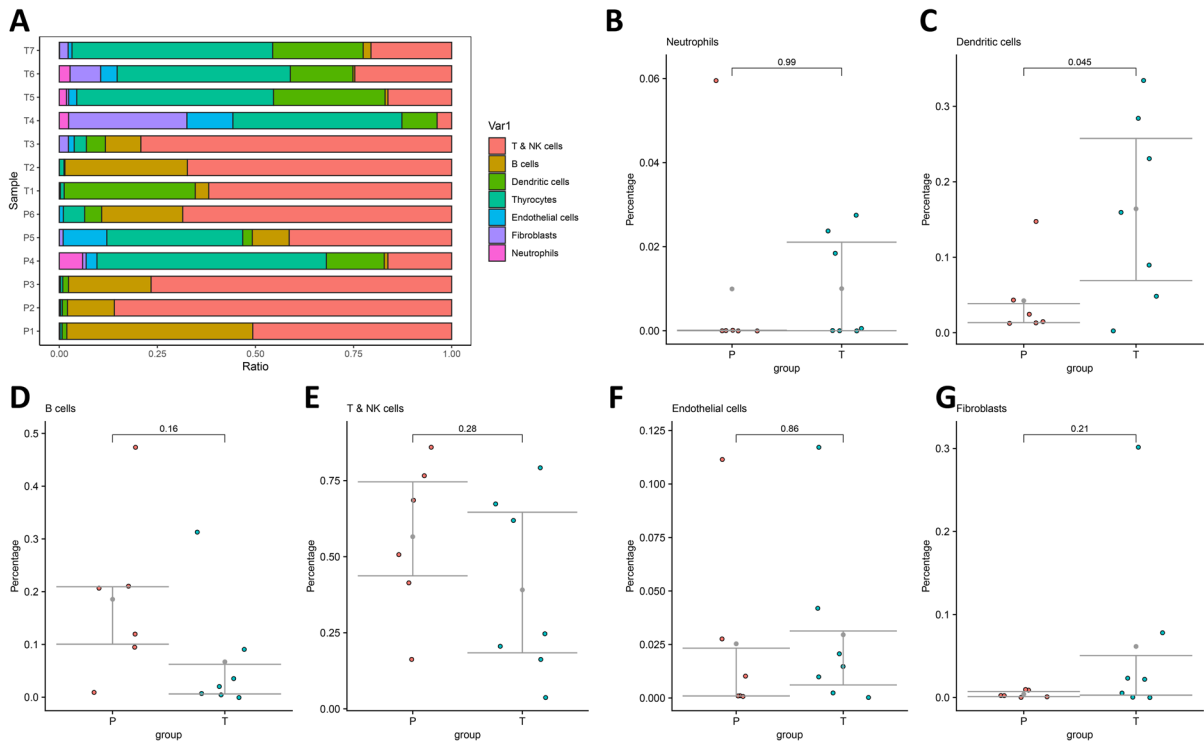


**Fig. 2** Analysis of Cell Proportions in Samples of THCA Patients' Tumor and Peritumor Tissues. Note: (A) Cell proportions in individual peritumor and tumor tissue samples; (B-G) Difference analysis of cell proportions in six peritumor tissues

and seven tumor tissue samples for Neutrophils, DCs, T & NK cells, B cells, Thyrocytes, Fibroblasts, and Endothelial cells, based on chi-square test for categorical data (adjacent tissue number (P) = 6, tumor tissue number (T) = 7)

CC, these genes were enriched in endocytic vesicles, ficolin-1-rich granules, vacuolar membranes, and lysosomal membranes. Furthermore, in MF, they were enriched in major histocompatibility complex (MHC) class II protein complex binding, MHC protein complex binding, immune receptor activity, and amide binding (Fig. 3B). Overall, DCs likely contribute to THCA initiation and progression via inflammatory and immune pathways.

DCs reside at the differentiation "Endpoint" in Pseudotime analysis

Pseudotime analysis was performed on seven tumor samples from the GSE184362 scRNA-seq dataset using Monocle2 (R package). Genes contributing to the pseudotime trajectory are shown in Fig. 4A. Dimensionality reduction with DDRTree ordered cells along trajectories in light of expression patterns of key genes (Fig. 4B). Pseudotime, calculated by Monocle2 based on cell gene expression information,

represents the order of time, with the root on the right and branches on the left (Fig. 4C). Additionally, the cell evolution is divided into three stages, with one significant branching point, as shown by State representation (Fig. 4D). We found that DCs are predominantly located at the branch endpoint, mainly in the State 2 stage (Fig. 4E). This was further validated by the expression trends of dendritic cell marker genes (HLA-DRA, HLA-DPB1, CST3, HLA-DPA1), which confirmed their pseudotemporal position at the "endpoint" (Fig. 4F).

Communication of DCs with various cell types in tumor tissues of THCA patients

Cellular communication analysis was then performed, which focuses on ligand-receptor interactions between cell types, highlighting communication dynamics within the TME. Initially, we performed cell-cell interaction analysis of 7 cell types using 14 common ligand-receptor

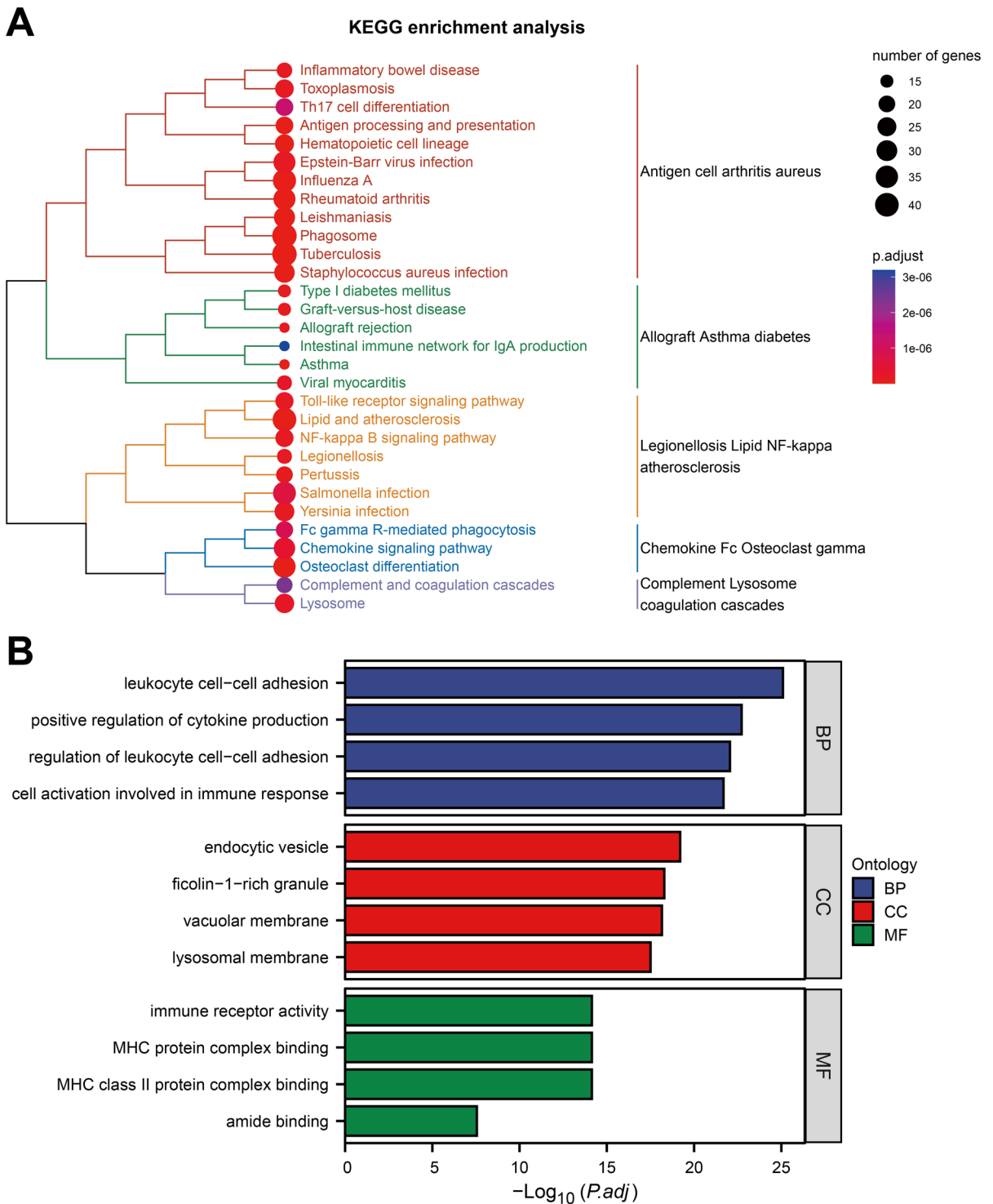


**Fig. 3** Enrichment Analysis of Genes Marked by DCs. Note: (A) KEGG pathway analysis of genes marked by DCs; (B) Enrichment analysis of GO terms for genes marked by DCs, including BP, CC, and MF

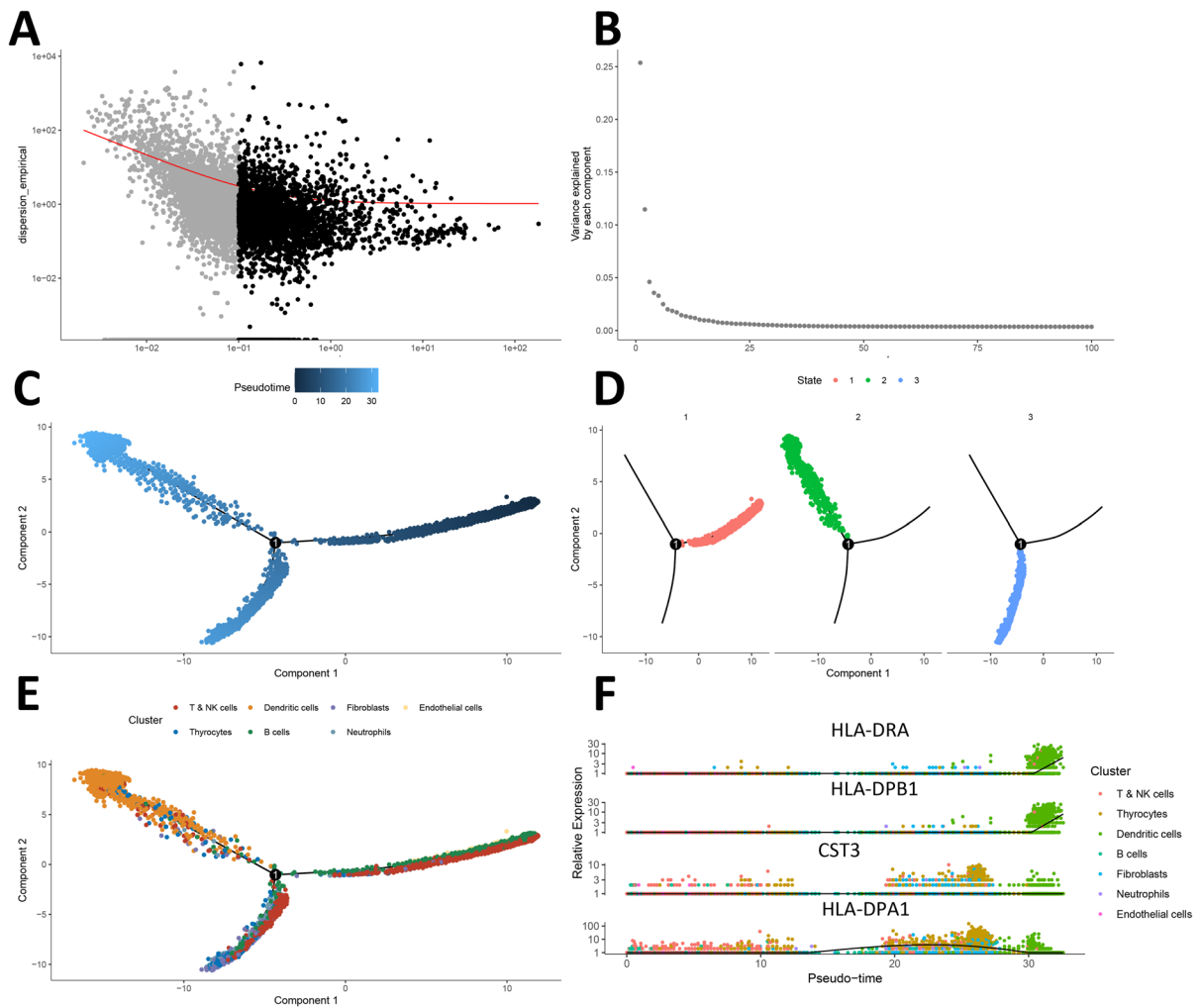


**Fig. 4** Pseudotemporal Analysis of scRNA-Seq Data. Notes: (A) Visualization of sorted genes used for subsequent dimension reduction, where each point represents a gene; (B) PCA, with the horizontal axis denoting the PC number and the vertical axis indicating the proportion of variance explained; (C)

Trajectory skeleton plot colored by Pseudotime; (D) Trajectory skeleton plot separately showing each branch (State); (E) Trajectory skeleton plot colored by cell type; (F) Expression changes of DC marker genes (HLA-DRA, HLA-DPB1, CST3, HLA-DPA1) over Pseudotime

pairs with the R software package CellCall. The results revealed that DCs had the highest number of interactions with other cells (Fig. 5A), primarily acting as cell receptors and responding to ligands from Neutrophils, T & NK cells, Thyrocytes, Fibroblasts, and other cells (Fig. 5B). Furthermore, analysis using the R software package CellChat demonstrated significant communication of DCs with other cells, involving signaling pathways such as Macrophage Migration Inhibitory Factor (MIF), SPP1, and Annexin (Fig. 5C). From

this, it can be seen that CellCall and CellChat analyses yielded concordant results, both confirming that DCs in the tumor tissue samples of THCA patients "communicate" with various other cell types. Combining the results of pseudotime analysis and cellular communication, it can be inferred that other stromal or immune cells in the tumor immune microenvironment may influence the differentiation and function of DCs, thereby further promoting the occurrence and development of THCA.

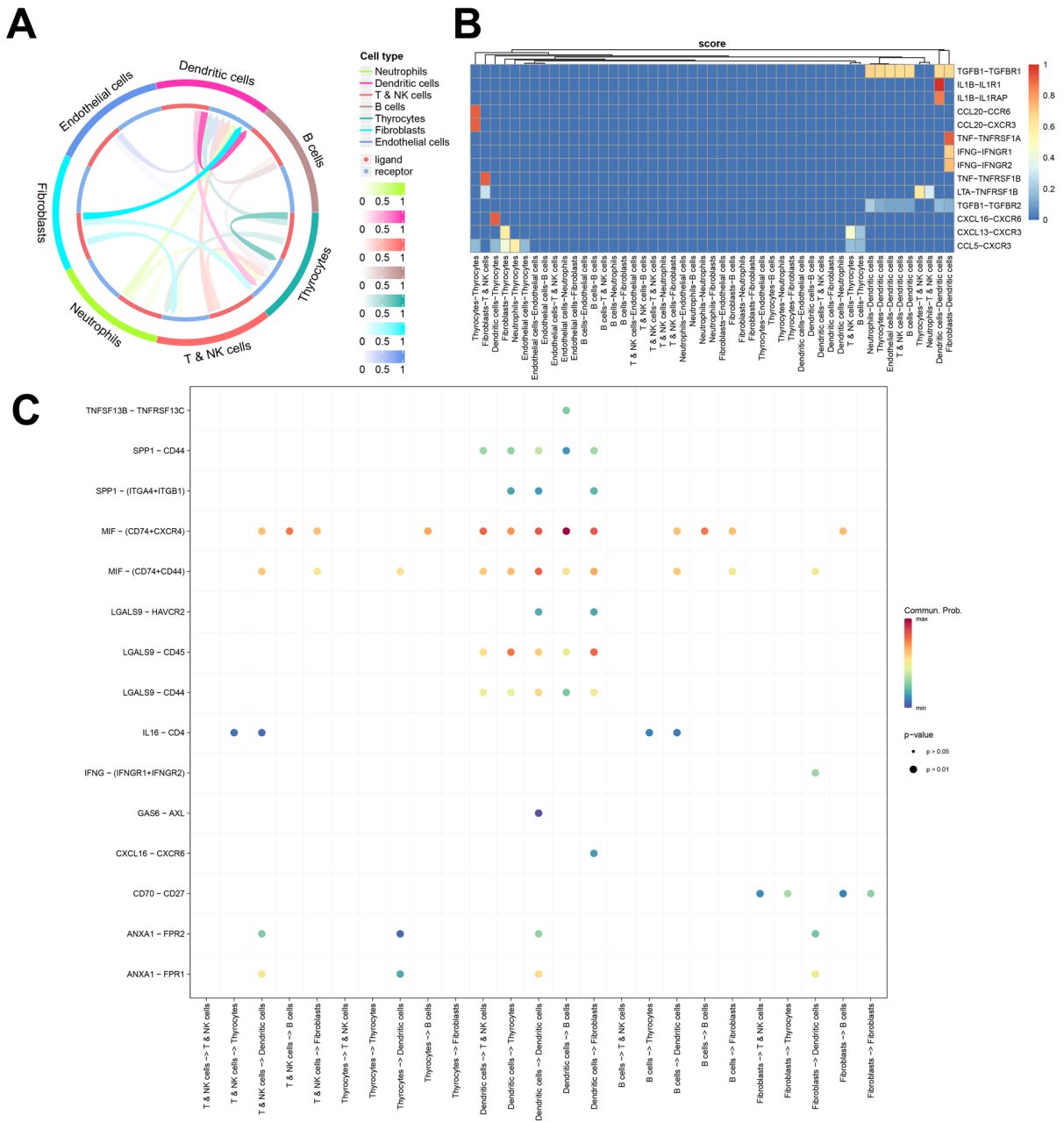


**Fig. 5** Analysis of Cellular Communication in scRNA-Seq Data from 7 Tumor Tissue Samples. Note: (A) Cell-cell communication network chord diagram; (B) Cell-cell communication network heatmap; (C) Cell-cell communication network bubble chart

Prognostic value of DC marker gene FPR1 in patients with THCA

Based on the ligand-receptor interactions in Fig. 5C, we extracted 41 ligand-receptor-related genes involved in the "communication" between DCs and

other cells, and intersected them with 833 dendritic cell marker genes, resulting in 16 candidate genes: SPP1, IL1B, CD74, IFNGR1, CXCL16, TNFSF13B, AXL, FPR1, IFNGR2, LGALS9, HAVCR2, CD4, TNF, CXCR3, GAS6, and CXCR4 (Fig. 6A). Survival analysis of the TCGA-THCA dataset revealed

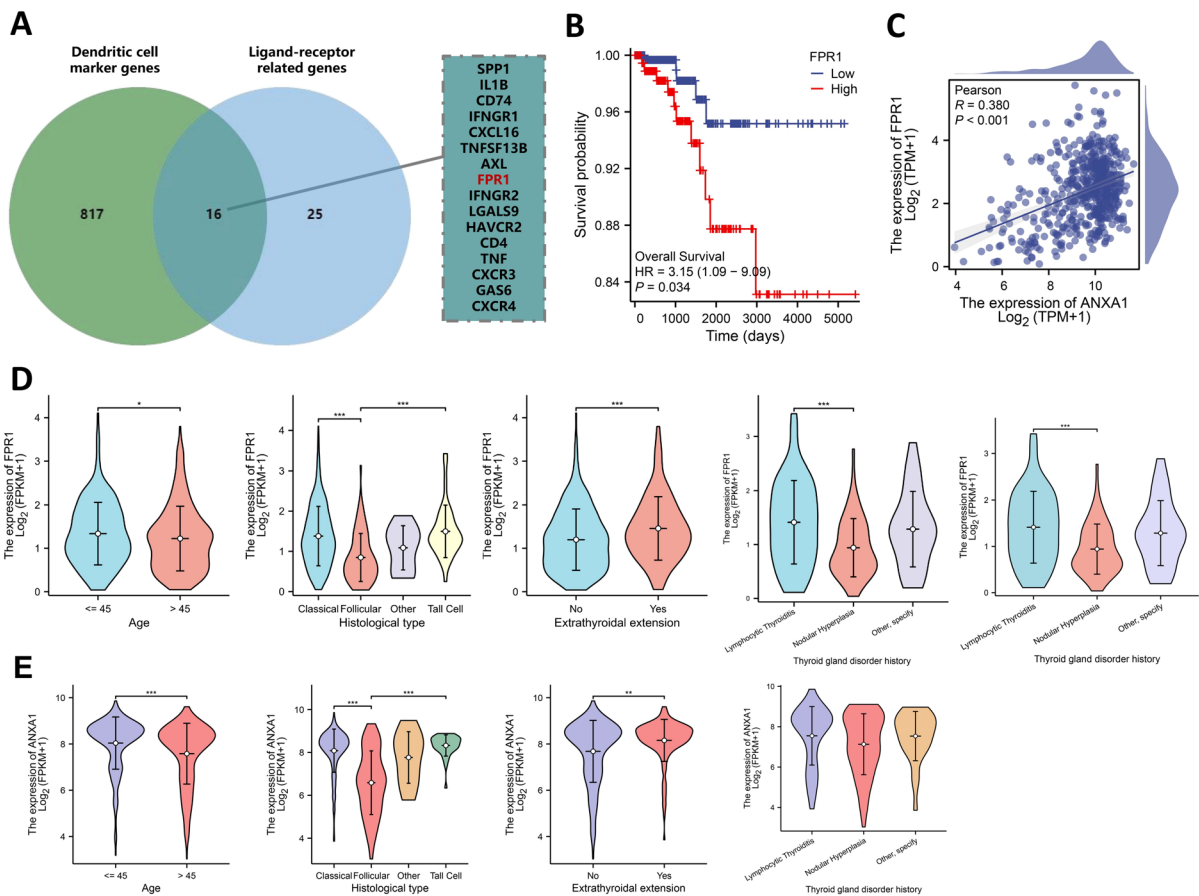


**Fig. 6** Analysis of the Prognostic Relevance of DC Marker Genes. Notes: (A) Venn diagram showing the intersection of ligand-receptor-related genes with DC marker genes; (B) Kaplan–Meier survival curve analysis of patients with high and low expression of FPR1; (C) Correlation analysis of FPR1 and ANXA1 expression in tumor tissue samples from THCA

patients; (D) Prognostic relevance analysis of FPR1 with various clinical indicators in tumor tissue samples from THCA patients; (E) Prognostic correlation analysis of ANXA1 with various clinical parameters in tumor tissue samples from THCA patients. n = 512

that only FPR1 was notably linked to overall survival, with high FPR1 expression correlating with poorer prognosis (Fig. 6B). The remaining 15 genes demonstrated no significant association with survival (Figure S4). In the THCA tissue samples from the TCGA-THCA dataset, FPR1 was significantly positively correlated with its corresponding ligand ANXA1 (Fig. 6C), further suggesting the link between FPR1 and ANXA1. Additionally, significant associations were identified between FPR1/ANXA1 expression and THCA clinical variables, such as Age, Thyroid gland disorder history, Histological type, and Extrathyroidal extension (Fig. 6D-E). This

suggests that the dendritic cell marker genes FPR1 and ANXA1 have prognostic value in THCA patients.

### Upregulation of FPR1 and ANXA1 expression in THCA tissues and cells

Initially, leveraging the TCGA-THCA dataset in conjunction with the GTEx dataset, we assessed the expression patterns of FPR1 and ANXA1 in THCA tissues. ANXA1 was evidently elevated in THCA tissues, whereas FPR1 showed no significant difference (Fig. 7A-B). To further explore this, we conducted a meta-analysis combining multiple THCA-related

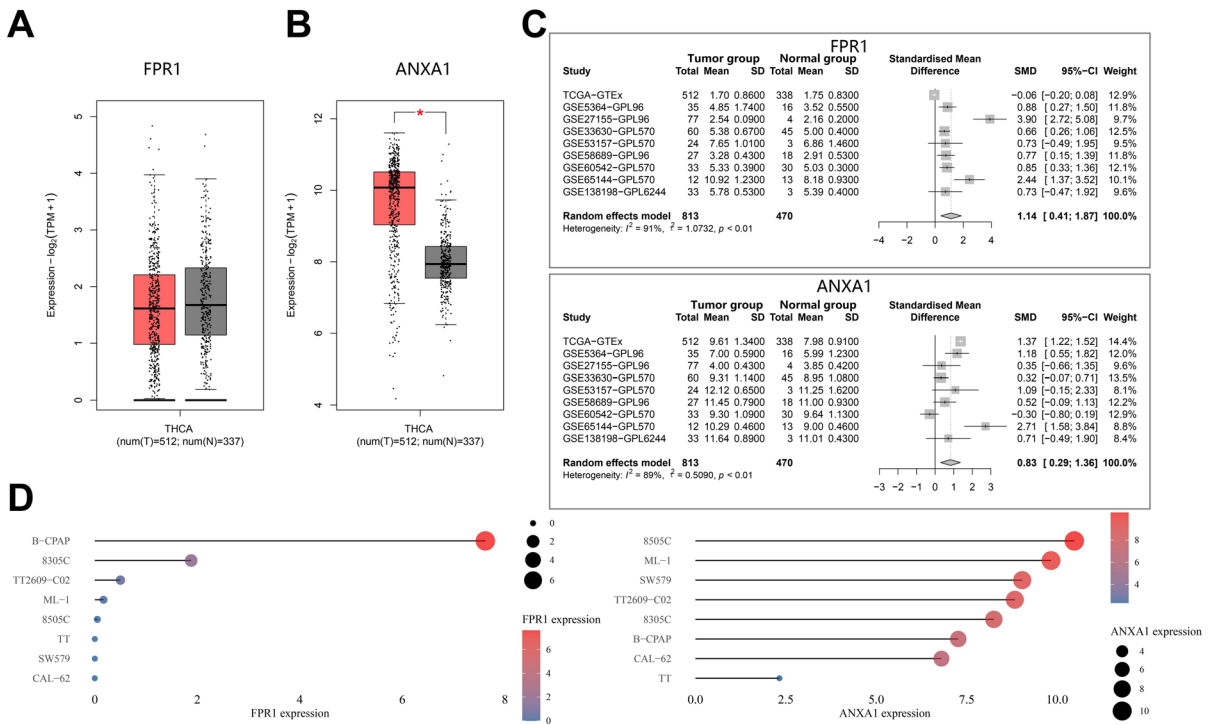


**Fig. 7** Differential Expression Analysis of FPR1 and ANXA1 in Tumor Tissues, Cells, and Normal Control Tissues of Patients with THCA. Note: (A) Expression levels of FPR1 mRNA in tumor tissues and normal control tissues of THCA patients (Tumor group, n = 512; Normal group, n = 337); (B) Expression levels of ANXA1 mRNA in tumor tissues and normal control tissues of THCA patients (Tumor group, n =

512; Normal group, n = 337); (C) Forest plot comparing the expression of FPR1 and ANXA1 in tumor samples (Tumor group) versus normal control tissue samples (Normal group) in patients with THCA; SMD denotes Standard Mean Difference, 95% CI denotes 95% confidence interval; (D) Expression analysis of FPR1 and ANXA1 in multiple THCA cell lines through the CCLE database

transcriptome datasets from GEO with TCGA-GTEX data.

Utilizing a random-effects model, the Meta-analysis results revealed that in THCA tissue samples, the expression levels of FPR1 (SMD = 1.14, 95%CI = 0.41 to 1.87) and ANXA1 (SMD = 0.83, 95%CI = 0.29 to 1.36) were distinctly higher than in samples of normal control tissues (Fig. 7C). Subgroup analysis based on detection methods (RNA-seq and array) demonstrated that while there was no notable difference in FPR1 expression employing the RNA-seq detection method, there was a notable difference in FPR1 expression utilizing the array detection method, indicating that different detection methods may impact the Meta-analysis results of FPR1 (Figure S5A). Furthermore, under both detection methods, ANXA1 expression in THCA tissue samples was evidently higher than the control tissues (Figure S5B). Sensitivity analysis conducted through a

leave-one-out approach demonstrated no significant changes in the results of each subgroup, demonstrating the methodological robustness of the meta-analytic conclusions (Figure S5C-D). Overall, the combined RNA-seq and array chip results for FPR1 and ANXA1 show that the chip detection results demonstrate higher consistency and significance for these two genes. Compared to normal control tissues, THCA tissue samples exhibited elevated FPR1 and ANXA1 levels.

Additionally, we queried the CCLE database to investigate the differential expression of FPR1 and ANXA1 in THCA cell lines. It was evident that FPR1 was distinctly expressed only in B-CPAP cells, whereas ANXA1 exhibited significant expression in multiple thyroid cell lines (Fig. 7D). This suggests that ANXA1 is broadly expressed in THCA cells, while the DC marker FPR1 may be expressed in immune cells such as DCs.

DC Involvement in THCA progression through the ANXA1-FPR1 signaling pathway

Utilizing the single-cell atlas of THCA constructed earlier, we examined the distribution of FPR1 and ANXA1 in seven cell types. The results revealed that FPR1 is predominantly expressed in DCs (Fig. 8A), while ANXA1 is distributed across all cell types

(Fig. 8B), consistent with the findings in Fig. 7D. Analysis of cellular communication indicated that DCs serve as a pivotal hub in the Annexin signaling pathway (Fig. 8C). Notably, DCs likely function primarily as the receiver, while neutrophils, T & NK cells, thyrocytes, and fibroblasts play roles as senders and influencers (Fig. 8D-E). Supported by evidence from the literature, ANXA1, a phospholipid-binding

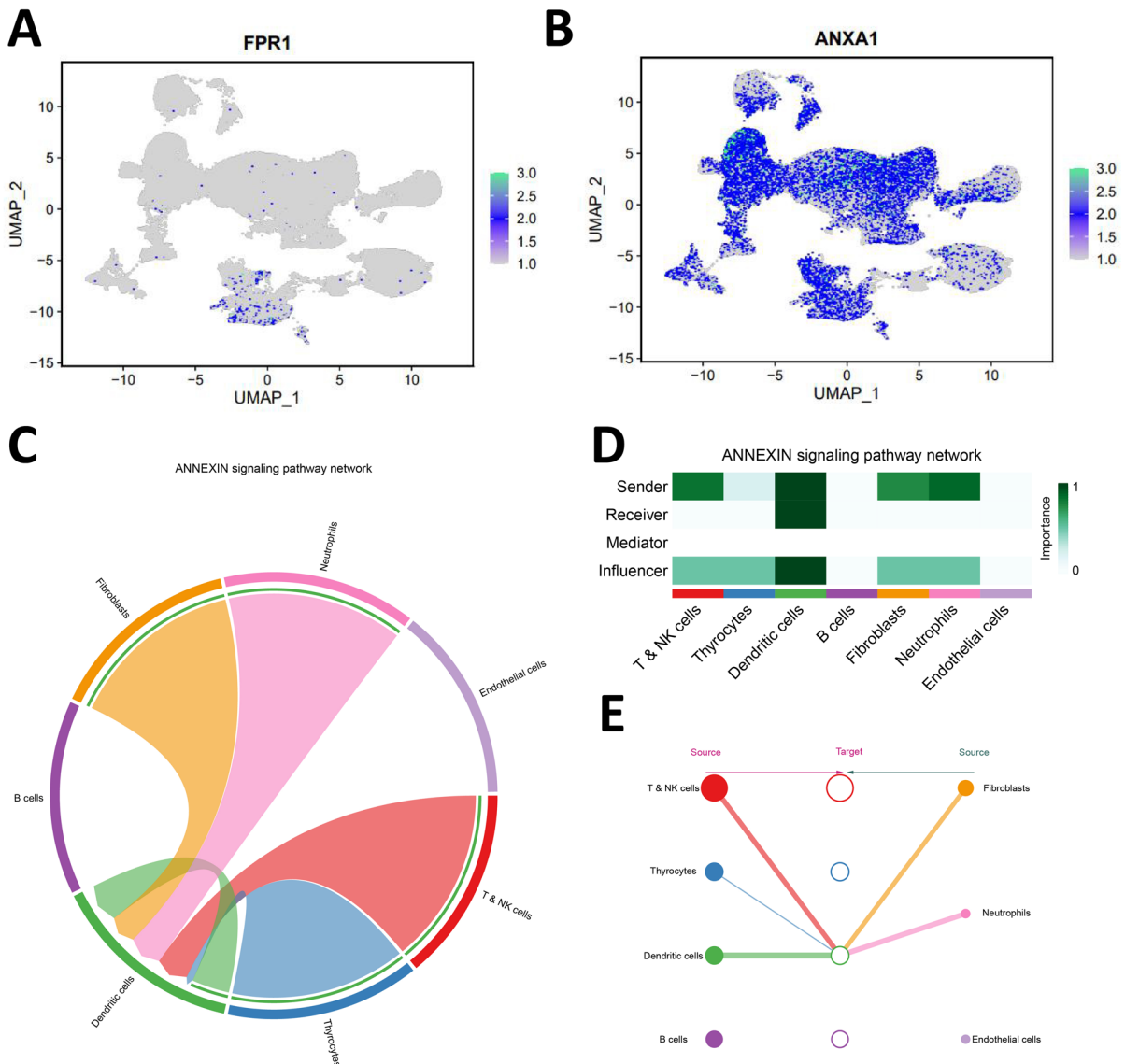
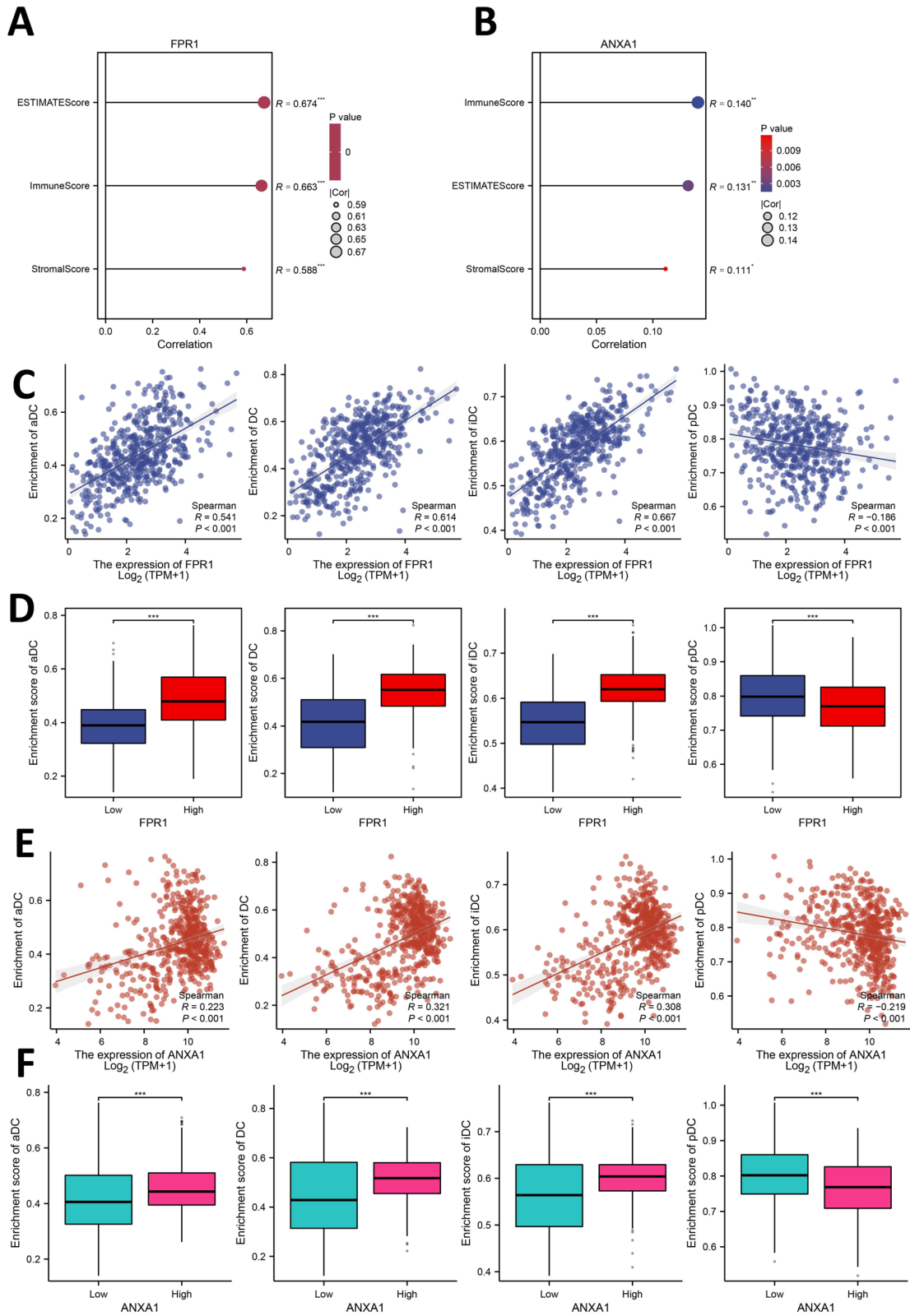


**Fig. 8** Distribution of FPR1 and ANXA1 in the Single-Cell Atlas and Analysis of Cellular Communication. Note: (A) Scatter plots showing the distribution of FPR1 in seven cell types; (B) Scatter plots showing the distribution of ANXA1 in seven cell types; (C) Network and chord diagram depicting

cell-cell communication in the Annexin signaling pathway; (D) Heat map illustrating cell-cell communication network in the Annexin signaling pathway; (E) Target map of cell-cell communication network in the Annexin signaling pathway



**◀Fig. 9** Immune Infiltration Analysis of FPR1 and ANXA1 in Tumor Tissues of THCA Patients. Note: (A) and (B) depict the lollipop graphs representing the correlation analysis of FPR1 and ANXA1 expression with StromalScore, ImmuneScore, and ESTIMATEScore. The size of the circles indicates the magnitude of the correlation coefficient, while different colors represent varying *P* values; (C) Scatter plot illustrating the correlation of FPR1 expression with the proportions of aDC, DC, iDC, and pDC infiltrates; (D) Discrepancies in the infiltration proportions of aDC, DC, iDC, and pDC between the high and low FPR1 expression groups; (E) Scatter plot showing the correlation between ANXA1 expression and the infiltration proportions of aDC, DC, iDC, and pDC; (F) Differences in the infiltration proportions of aDC, DC, iDC, and pDC between high and low ANXA1 expression groups. \* denotes  $P < 0.05$ , \*\* denotes  $P < 0.01$ , \*\*\* denotes  $P < 0.001$ ,  $n = 512$

protein, belongs to the Annexin protein family. FPR1 is a G protein-coupled receptor that, when activated, interacts with ANXA1 to form the ANXA1-FPR1 complex. This complex triggers downstream signaling events within the cell, including calcium ion release, activation of protein kinases, and transcription factors, thereby regulating the activation, chemotaxis, and inflammatory responses of immune cells (Vecchi et al. 2018, 2022). Therefore, we posit that the release of ANXA1 from neutrophils, T & NK cells, thymocytes, and fibroblasts binds to the FPR1 marker gene on DCs, influencing their function and ultimately modulating the TME to promote THCA initiation and progression.

#### Influence of FPR1 on DC maturation and activation

Following the application of the ESTIMATE algorithm, we calculated StromalScore, ImmuneScore, and ESTIMATEScore for THCA samples and analyzed their correlation with FPR1 and ANXA1 expression. FPR1 was notably linked with all three scores (Fig. 9A), while ANXA1 showed weaker correlations (Fig. 9B). Single sample gene set enrichment analysis (ssGSEA) analysis validated a notable positive correlation between FPR1 and ANXA1 expression and the infiltration of activated DCs, DCs, and immature DCs, while the correlation with plasmacytoid DCs was weaker (Fig. 9C-E). In light of median expression values of FPR1 and ANXA1, THCA samples were categorized into high and low expression groups. Differential analysis of DC subsets (aDC, DC, iDC, pDC) confirmed these findings (Fig. 9D-F).

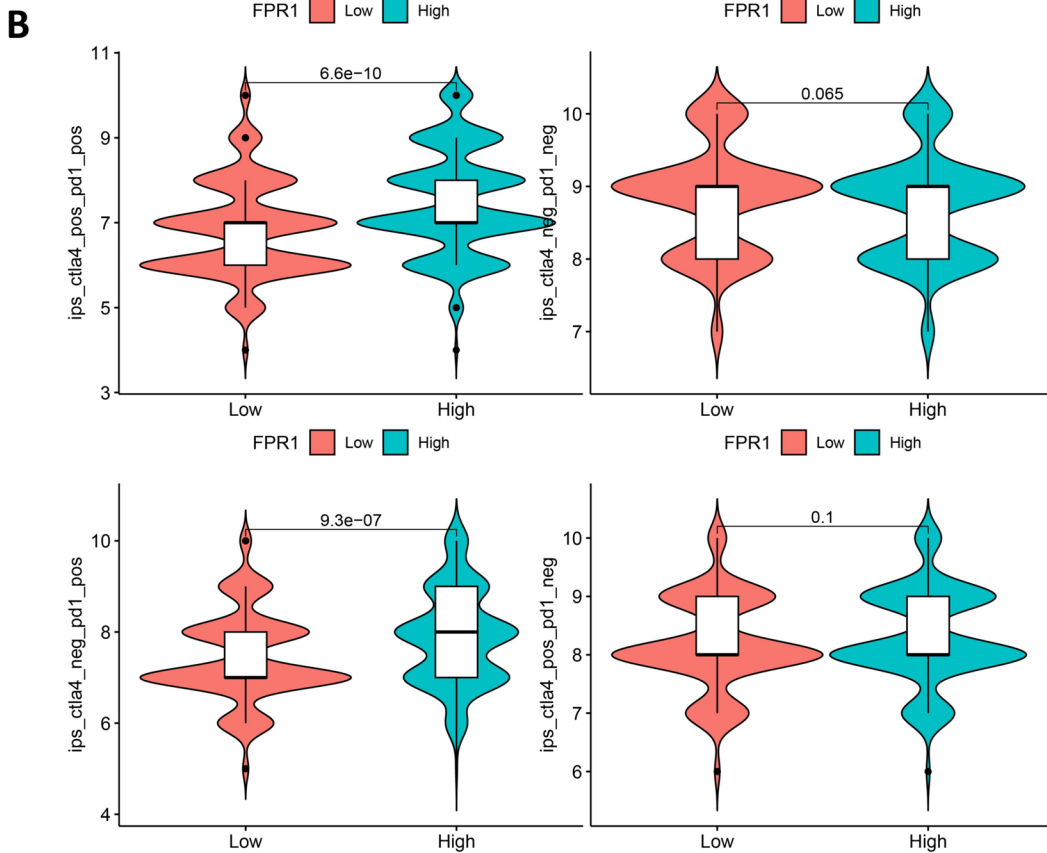
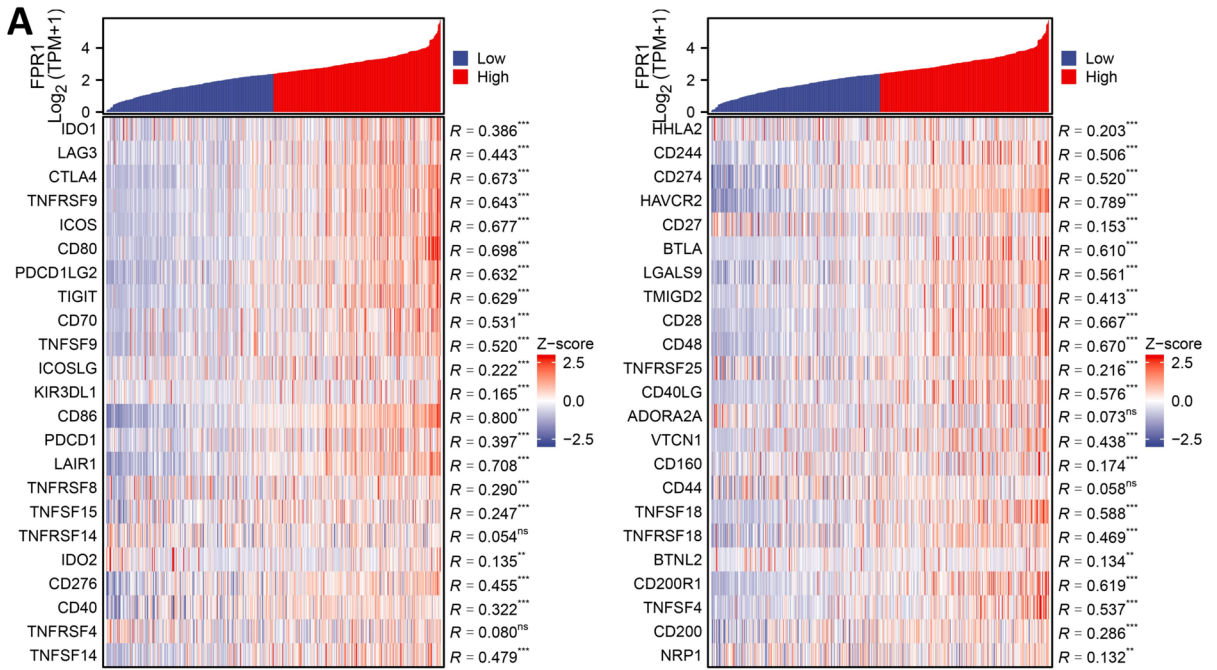
#### FPR1 as a potential guide for immunotherapy in THCA patients

Here, a correlation analysis between FPR1 and common immune checkpoints was done with the results demonstrating a significant positive correlation between them (Fig. 10A). Subsequently, we accessed immunotherapy-related data on THCA patients from the TCIA database. The Immunotherapy scores were plotted on the y-axis, where higher scores indicate a better response to Immunotherapy. Relative to the low FPR1 expression group, those with high expression showed enhanced responses to PD-1 inhibitors or a combination of CTLA4 and PD-1 inhibitors (Fig. 10B). Therefore, it can be inferred that THCA patients with high FPR1 expression may indicate potential benefit from ICIs, either alone or in combination.

ANXA1 May facilitate proliferation, migration, and invasion of THCA cells by interacting with DC marker gene FPR1

Bioinformatics analysis revealed a significant elevation in ANXA1 and FPR1 expression in THCA tissues, accompanied by enhanced activation and infiltration of DC cells. Furthermore, literature reports suggest that the interaction between ANXA1 and its receptor FPR1 inhibits TNF- $\alpha$ -induced DC maturation, thereby modulating their activity and function (Baracco et al. 2019; Min et al. 2011). To further validate this conclusion, we plan to conduct relevant experiments under cell culture conditions.

Initially, we validated the interaction between ANXA1 and FPR1 in DCs. Bidirectional immunoprecipitation results showed that ANXA1 could specifically bind to FPR1 (Fig. 11A). Subsequently, we modulated the expression of ANXA1 and FPR1 in DC cells through lentiviral transduction. Western blot results displayed (Fig. 11B) a notable decline in ANXA1 and FPR1 expression levels following sh-ANXA1 treatment. In the group overexpressing FPR1 alongside silenced ANXA1 (sh-ANXA1 + oe-FPR1 group), there was a notable elevation in FPR1 expression levels, while ANXA1 expression levels remained relatively unchanged. Therefore, cells infected with the lentivirus can be utilized for subsequent experiments. Subsequently, we analyzed the effects of ANXA1 knockdown and FPR1 overexpression on



◀**Fig. 10** Correlative Analysis of FPR1 with Common Immune Checkpoints and Immunotherapy Analysis. Note: (A) Correlative Analysis of FPR1 with Common Immune Checkpoints (n = 512); (B) Differential Analysis of IPS between FPR1 High-expression and Low-expression Groups (n = 501)

DC maturation, phagocytic ability, and CD8 + T cell stimulatory capacity. Flow cytometry results indicated that sh-ANXA1 treatment brought about increased expression of CD86 and CD1a, suggesting that ANXA1 knockdown promoted DC maturation (Fig. 11C). The phagocytic ability of DC cells co-cultured with Detran was significantly higher in the sh-ANXA1 + oe-NC group relative to respective control (Fig. 11C). Additionally, the CCK-8 assay evaluating CD8 + T cell proliferation with different DC co-cultures demonstrated a significantly higher proliferation capacity following sh-ANXA1 treatment (Fig. 11D). Consistent with our expectations, overexpression of FPR1 reversed the promoting effects of ANXA1 knockdown on DC cell activity, phagocytic ability, and CD8 + T cell stimulatory capacity (Fig. 11C-D).

We next employed cell co-culture techniques to stimulate CD8 + T cells with DCs, followed by further co-cultivation with TPC-1 cells to assess relevant indicators. CCK-8 and colony formation assays showed a notable decline in TPC-1 and B-CPAP cell proliferation following sh-ANXA1 treatment (Fig. 11E-G). Silencing ANXA1 in DCs, combined with FPR1 overexpression, reversed the proliferation inhibition in TPC-1 cells. Transwell assays revealed diminished migration and invasion in TPC-1 cells following sh-ANXA1 treatment (Fig. 11H-I), which were reversed by FPR1 overexpression in DCs. These results suggest that ANXA1 interacts with FPR1 on DCs to regulate TPC-1 cell proliferative, migrative, and invasive potentials.

**Inhibiting the Interaction Between ANXA1 and FPR1 May Reduce DC Infiltration and the Development of THCA in a Mouse Model.**

To further validate the effects of ANXA1 and FPR1 on DC activity in THCA, we established a subcutaneous THCA tumor model in mice. Tumor observations and volume measurements revealed that the tumor size and morphology were evidently diminished following sh-ANXA1 treatment. Additionally, after FPR1 overexpression (sh-ANXA1 + oe-FPR1 group), the growth inhibition of subcutaneous tumors in mice was reversed (Fig. 12A-B). This preliminary

finding suggests that inhibiting ANXA1 and FPR1 can suppress THCA progression in vivo (Fig. 12C).

Furthermore, we constructed a lung metastasis model of THCA, following assessment of the expression levels of the DC infiltration marker BATF3 in tissue samples from the subcutaneous THCA tumor model. The results confirmed that, relative to the sh-NC + oe-NC group, the sh-ANXA1 + oe-NC group showed evidently higher mRNA and protein levels of the DC marker BATF3, while these levels were reduced in the sh-ANXA1 + oe-FPR1 group (Fig. 12D-F). Immunofluorescence staining confirmed lower expression of ANXA1 and FPR1 in the sh-ANXA1 + oe-NC group, with further reduction in the sh-ANXA1 + oe-FPR1 group (Fig. 12G). These findings suggest that inhibiting ANXA1 and FPR1 promotes DC infiltration in THCA tissue.

Flow cytometry showed a notable elevation in BATF3/CD1a double-positive cells in the sh-ANXA1 + oe-NC group, indicating increased DC infiltration. FPR1 overexpression in the sh-ANXA1 + oe-FPR1 group diminished BATF3 expression and DC infiltration (Fig. 12H). T cell infiltration analysis revealed higher CD4 + and CD8 + T cell levels in the sh-ANXA1 + oe-NC group, while FPR1 overexpression led to a remarkable decline in T cell infiltration (Fig. 12I).

These results indicate that inhibiting the interaction between ANXA1 and the DC marker gene FPR1 in the TME reduces DC activity, ultimately suppressing the occurrence and development of THCA.

## Discussion

In light of the results obtained, we preliminarily conclude that in the TME, the binding of ANXA1 with the DC marker gene FPR1 influences the maturation and activation of DCs, ultimately accelerating THCA (Fig. 13).

In previous studies, the roles of various cells in the TME of THCA have gradually gained attention (Zhou et al. 2023; Ferrari et al. 2019; Li et al. 2022a, b; Garcia-Alvarez et al. 2022). Despite extensive research focusing on T cells, neutrophils, and other cells, the specific role of DCs in THCA remains unclear (Xie et al. 2020; Jin et al. 2021; Gong et al. 2020). This study delves deep into how DCs participate in and reshape the TME of THCA through scRNA-seq and

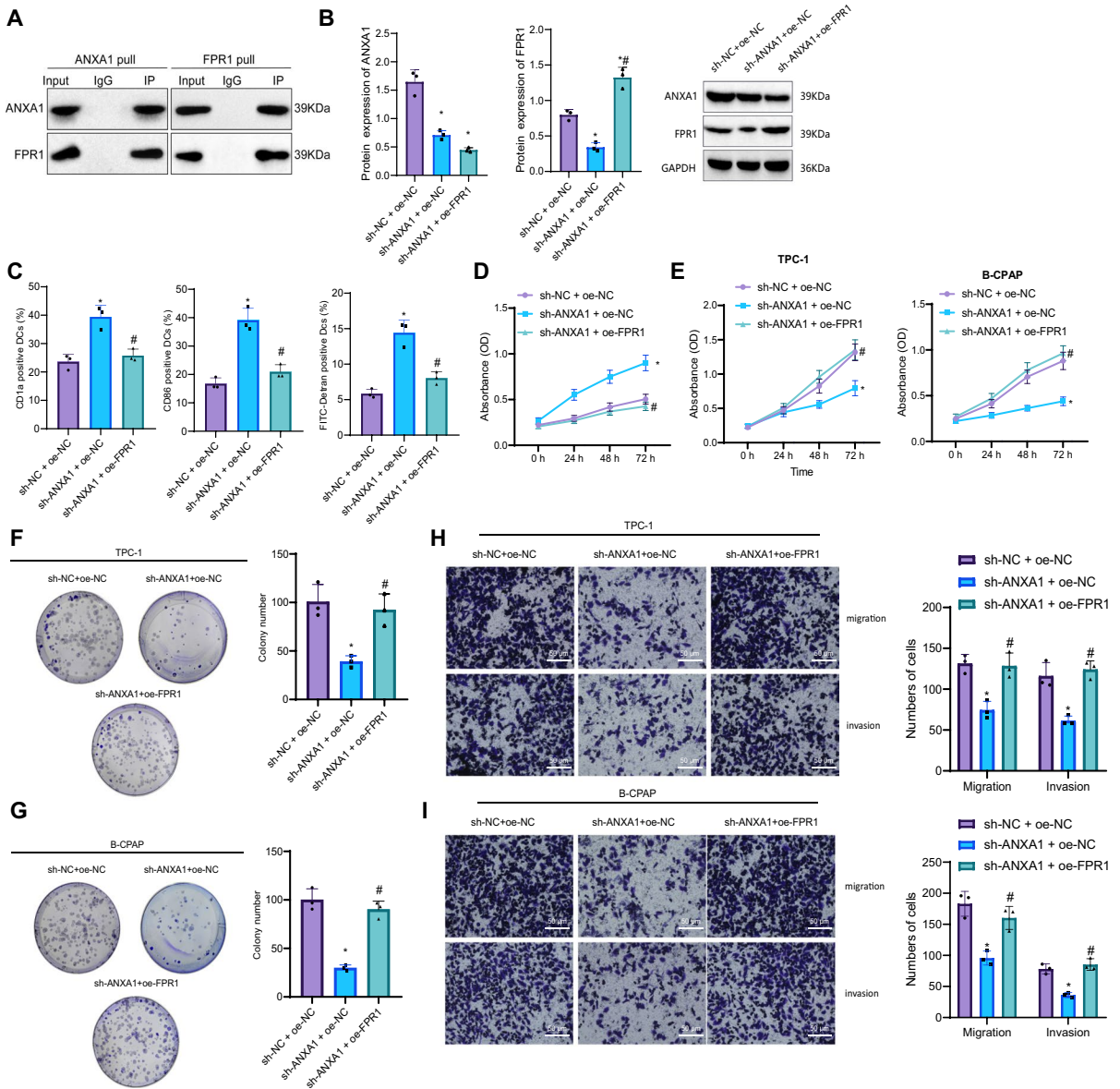


**Fig. 11** The Impact of ANXA1 and FPR1 Interaction on DC Activity and Malignant Behavior of THCA Cells. Note: (A) Immunoprecipitation assay to detect the interaction between ANXA1 and FPR1; (B) Western blot validation of ANXA1 and FPR1 lentivirus construction in DC cells; (C) Flow cytometry analysis of DC cell markers CD1a and CD86, as well as the phagocytic capacity of DCs for FITC-Dextran; (D) CCK-8 experiment to assess the proliferation ability of CD8 + T cells in each group; (E) CCK-8 assay to measure the proliferation ability of TPC-1 cells and B-CPAP cells in each group;

(F) Clonogenic assay to evaluate the clonogenic potential of TPC-1 cells in each group; (G) Clonogenic assay to measure the clonogenic ability of B-CPAP cells in different groups; (H) Transwell assay to determine the migration and invasion abilities of TPC-1 cells in each group, Scale bar = 50µm; (I) Transwell assay to measure the migration and invasion ability of B-CPAP cells in different groups, Scale bar = 50µm. \* indicates  $P < 0.05$  compared to the sh-NC + oe-NC group, # indicates  $P < 0.05$  compared to the sh-ANXA1 + oe-NC group, and all cell experiments were performed in triplicate

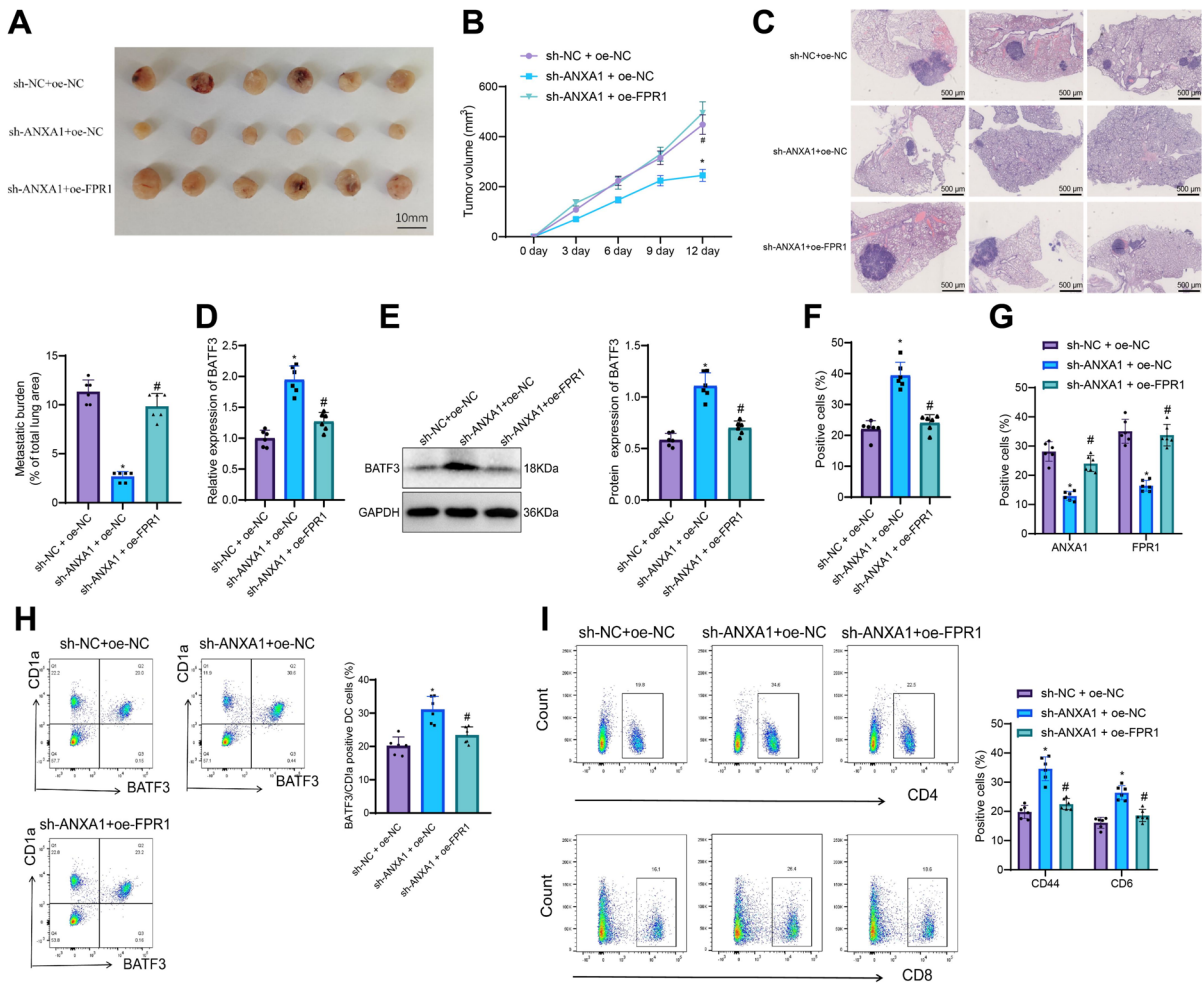


**Fig. 12** Regulation of ANXA1 and FPR1 on DC Cell Infiltration in a Mouse Model and its Impact on THCA. Notes: (A) Representative images of tumors in different groups of mice; (B) Statistical analysis of tumor volumes in mice; (C) Mouse lung metastasis model, HE staining of lung tissues, and statistics of tumor metastatic burden; (D) mRNA changes of the DC cell infiltration marker BATF3 in subcutaneous tumors of different mouse groups as detected by RT-qPCR; (E) Protein changes of the DC cell infiltration marker BATF3 in subcutaneous tumors of different mouse groups as detected by Western blot; (F) Immunofluorescence staining showing the protein

expression of the DC cell infiltration marker BATF3 in subcutaneous tumors of different mouse groups, with a scale bar of 10 μm; (G) Immunofluorescence staining showing the protein expression of ANXA1 and FPR1 in subcutaneous tumors of different mouse groups, with a scale bar of 500 μm; (H) Flow cytometry analysis of DC cell infiltration in different groups of mice with subcutaneous tumors; (I) Flow cytometry analysis of CD4 + and CD8 + T cell infiltration in different groups of mice with subcutaneous tumors. \* indicates  $P < 0.05$  compared to the sh-NC + oe-NC group, # indicates  $P < 0.05$  compared to the sh-ANXA1 + oe-NC group, with  $n = 6$  in each group

transcriptomic RNA sequencing data analysis (Tian et al. 2023).

In previous research, DCs have been recognized as key cells in regulating the TME (Li et al. 2022a, b; Wculek et al. 2019; Peng et al. 2021). Our study further indicate that among the analyzed single-cell transcriptome data, only DCs exhibit a significant difference in proportion between THCA tissue and

corresponding adjacent tissue samples. This highlights the potential central role of DCs in THCA development, which is in line with the findings of Gulubova et al., who also validated the crucial role of DCs in THCA development (Gulubova et al. 2014).

The interaction between ANXA1 and FPR1 are vital in modulating the TME, particularly affecting the maturation and activation of DCs (Le Naour

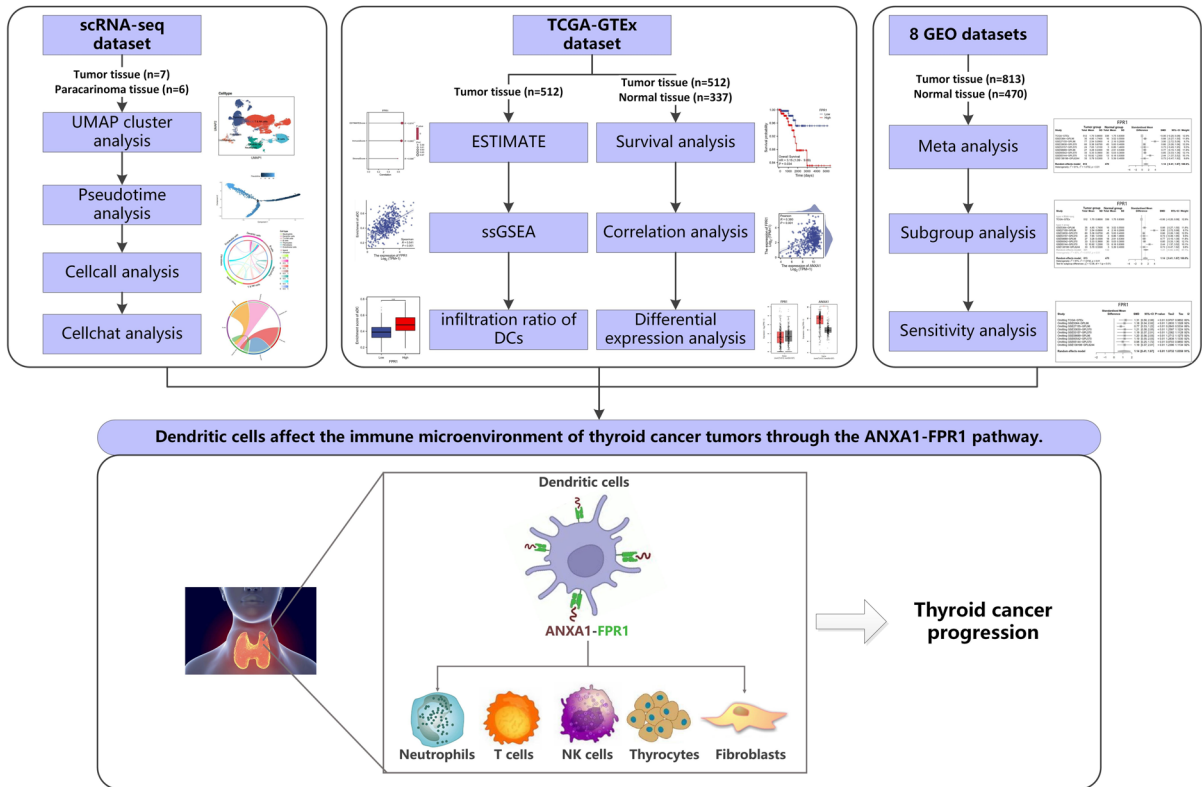


**Fig. 13** Molecular Mechanism Illustration of ANXA1 Binding to the DC Marker Gene FPR1 in the TME, Influencing DC Maturation and Activation, Ultimately Promoting the Occurrence and Development of THCA

et al. 2021). Previous studies have documented that ANXA1 facilitated tumor cell invasion, migration, and immune escape in various cancers, with FPR1 as its main receptor playing a significant role in these processes (Foo et al. 2019; Araújo et al. 2021). However, there is still limited research and reporting on the specific mechanism of this signaling axis in THCA. Recent studies have started to focus on the role of ANXA1 and FPR1 in modulating the immune microenvironment, especially within DCs. DCs, as crucial antigen-presenting cells in the immune system, directly impact T-cell activation and the establishment of immune responses based on their maturation and activation status. The interaction between ANXA1 and FPR1 regulates the functions of DCs through various aspects, such as intracellular calcium signaling, cytokine release, and cell chemotaxis (Feng et al. 2020).

In THCA, this interaction may alter the antigen-presenting ability of DCs and modulate the cytokine environment, further influencing T-cell reactivity

and tumor cell immune evasion. This study, through bioinformatics analysis and experimental validation, reveals how they interact with DCs, thereby propelling the development of THCA. The interaction between ANXA1 and FPR1 in the THCA TME inhibits the maturation and activation of DCs. Analysis of scRNA-seq data revealed elevated ANXA1 and FPR1 expression in DCs in THCA tissues compared to adjacent tissues, with both negatively correlating with tumor invasiveness and patient prognosis. These findings align with prior reports showing that exosomal ANXA1 promotes macrophage M2 polarization in PTC (Liu 2024). This further suggests that ANXA1, through its interaction with immune cells, may critically shape the immune microenvironment of THCA and represent a potential immunotherapeutic target. Additionally, other studies provide important supplementary evidence showing that ANXA1 is highly connected to the regulation of the immune microenvironment in PTC (Chen et al. 2022a, b), reinforcing its role in immune modulation. While similar

conclusions have not been found in THCA-related studies, Vecchi et al. discovered that inhibiting the ANXA1/FPR1 autocrine axis effectively reduced the proliferation and migration of breast cancer cells, evident in cell culture and animal studies (Vecchi et al. 2018). This finding further supports the reliability of our results. Such findings offer new insights for Immunotherapy in THCA, suggesting that enhancing the immune activation function of DCs and inhibiting tumor development may be achieved through modulating the expression or function of ANXA1 and FPR1.

The strong positive correlation between FPR1 and most immune checkpoints presents a novel strategy for Immunotherapy in THCA. Patients with high FPR1 expression may benefit from ICIs, providing a more targeted direction for future therapeutic strategies. Through *in vivo* experiments, this study demonstrates that silencing ANXA1 effectively promotes the maturation of DCs, thereby inhibiting the tumorigenic capacity and tumor size of THCA cells. This offers empirical support for considering ANXA1 as a potential therapeutic target, differing from previous studies that primarily focused on molecular biomarkers. Overall, this research unveils the crucial role of DCs in the TME of THCA, emphasizing the significance of ANXA1 and FPR1. This offers new insights into THCA pathogenesis and a strong rationale for future therapeutic modalities.

This study employed advanced scRNA-seq technology to comprehensively reveal the cellular composition of the immune microenvironment in THCA. Pseudotime analysis, a scRNA-seq method, was used to explore dynamic changes in cell states. In tumor immunology research, this approach can reveal the developmental trajectory and functional changes of DCs during tumor progression (Qiu et al. 2017). In this study, pseudotime analysis indicated that DCs were located at the branch endpoint, suggesting further differentiation of DCs and indicating that they were in a fully mature state. Additionally, cellular communication analysis, based on known receptor-ligand interactions, predicted the interactions between various cell types (Jin et al. 2024), suggesting that DCs interact with multiple other cell types. Previous evidence has pinpointed that the differentiation and function of DCs may be influenced by other cell types, which can impact DC maturation and function through the secretion of cytokines, metabolic

products, or direct cell-to-cell contact (Grandclaudon et al. 2019; Li et al. 2018). In this study, FPR1 and its ligand gene ANXA1 were evidently linked to the survival of THCA patients, implying that they may serve as new therapeutic targets. Specifically, the significant positive correlation between FPR1 and most immune checkpoints provides a clue for its potential as a novel immunotherapy target. Validation of the roles of ANXA1 and FPR1 in THCA through *in vivo* and *in vitro* experimentations further enhances the clinical relevance of these findings, offering guidance for future patient treatment strategies.

Furthermore, differences were observed between the RNA-seq and array results for FPR1, which may be due to sample variations or differences in sequencing methods. RNA-seq does not rely on pre-designed probes, allowing for the detection of new transcripts, gene fusions, single nucleotide polymorphisms (SNPs), and insertions/deletions (indels), which cannot be captured by traditional gene chips (Wang et al. 2009). On the other hand, gene chips are more established, easier to analyze, and often less expensive for large-scale sample analyses. This suggests that both sequencing methods have their advantages, but one should not conclude that chip technology is superior to RNA-seq.

In this study, we observed a reduction in FPR1 expression after ANXA1 knockdown, suggesting a regulatory relationship between ANXA1 and FPR1 expression. Previous studies have indicated that ANXA1 may indirectly regulate FPR1 expression in the TME by influencing immune cell functions, thus affecting tumor immune evasion and progression. ANXA1 is known to interact with different receptors, such as FPR2/ALX, and is involved in regulating platelet function, promoting the resolution of inflammation, and playing a role in ischemia-reperfusion injury (Senchenkova et al. 2019). ANXA1 overexpression correlates with unfavorable prognosis across several malignancies, including breast, lung, and melanoma, where it promotes immune evasion through regulating PD-L1 expression via its interaction with PARP1 and Stat3 activity (Xiao et al. 2023). Additionally, our unexpected finding showed that the formation of the ANXA1-FPR1 complex was reduced after ANXA1 knockdown, and FPR1 overexpression did not restore ANXA1 complex formation as seen in the shNC +oe-NC group. This could be due to the presence of alternative ligands for FPR1, such as

peptides with N-formylated methionine, serum amyloid A (SAA), peptides derived from the HIV virus, the virulence factor of *Yersinia pestis*, amyloid- $\beta$ , and lipid ligands like LXA4 and Resolvin D1 (Zhuang et al. 2022). These findings suggest that FPR1 may have alternative signaling partners or pathways that mediate its antitumor effects. Therefore, the compensatory effects observed in animal experiments might be due to the activation of alternative signals, which may be absent *in vitro*, leading to discrepancies between cell culture and animal studies.

Although this study utilized samples from different databases, such as GEO and TCGA, providing valuable data support, the limited geographical scope and sample size may restrict the generalizability and applicability of the findings. Future research should include more multi-center samples to improve the extrapolation of results and validate whether these findings are applicable to a broader population. This study preliminarily reveals the significance of ANXA1 and FPR1 in DC maturation and activation, but the specific molecular mechanisms remain unclear. For instance, more fundamental experiments are needed to explore how this interaction affects DC maturation and other immune regulatory processes. While the study suggests that FPR1 and ANXA1 may be new therapeutic targets, questions remain about how to effectively and safely target these molecules in treatment. Future research should focus on the drug feasibility, side effects, and therapeutic windows for targeting these molecules, particularly in the context of multimodal therapies. Given these findings, advancing FPR1 and ANXA1 toward clinical application appears both timely and promising. These trials will be a key step in translating laboratory research into clinical application.

Despite comparable FPR1 expression between two studied tissues, elevated levels in tumors were linked to poorer patient prognosis. This suggests that FPR1 expression varies significantly in THCA tissues, and higher FPR1 expression may be associated with tumor heterogeneity, contributing to poorer patient outcomes. The cell lines used in this study mainly represented papillary THCA, which is the most common subtype of THCA. However, it is recognized that our findings regarding the roles of ANXA1 and FPR1 may not be entirely applicable to other THCA subtypes, such as follicular THCA, medullary THCA, and anaplastic THCA. The experiments were

primarily based on papillary THCA cell lines (e.g., TPC-1, B-CPAP), which may limit the generalizability of our conclusions to other subtypes. Future studies should conduct validation experiments in different THCA subtypes to determine whether the ANXA1-FPR1 axis plays a similarly important role. By doing so, we hope to broaden the clinical relevance of these findings and explore the potential of ANXA1 and FPR1 as therapeutic targets for a wider range of THCA subtypes. Combining the findings from this study with other known treatment modalities may help develop more effective combination therapy strategies.

By elucidating the immune landscape of THCA, this study uncovers promising avenues for future immunotherapeutic strategies.

**Acknowledgements** None.

**Author Contributions** Hongwei Jiang and Lirun Kuang conceived and designed the study. Tianyi Zhang and Lirun Kuang conducted the experiments and analyzed the data. Hongwei Jiang performed the meta-analysis and contributed to data interpretation. Tianyi Zhang assisted in the preparation of the manuscript. Xupeng Zhao supervised the study and revised the manuscript for critical intellectual content. All authors have read and approved the final manuscript.

**Funding** This study was supported by Liaoning Provincial Natural Science Foundation (2014021094).

**Data availability** The datasets generated and/or analyzed during the current study are not publicly available due to privacy and confidentiality agreements with the participants but are available from the corresponding author on reasonable request.

**Declarations**

**Ethical approval** All animal experiments were approved by the Animal Ethics Committee of China Medical University (No. CMUXN2023070).

**Competing interest** The authors declare no competing interests.

**Open Access** This article is licensed under a Creative Commons Attribution-NonCommercial-NoDerivatives 4.0 International License, which permits any non-commercial use, sharing, distribution and reproduction in any medium or format, as long as you give appropriate credit to the original author(s) and the source, provide a link to the Creative Commons licence, and indicate if you modified the licensed material. You do not have permission under this licence to share adapted material

derived from this article or parts of it. The images or other third party material in this article are included in the article's Creative Commons licence, unless indicated otherwise in a credit line to the material. If material is not included in the article's Creative Commons licence and your intended use is not permitted by statutory regulation or exceeds the permitted use, you will need to obtain permission directly from the copyright holder. To view a copy of this licence, visit <http://creativecommons.org/licenses/by-nc-nd/4.0/>.

## References

- Araújo TG, Mota STS, Ferreira HSV, Ribeiro MA, Goulart LR, Vecchi L. Annexin A1 as a Regulator of Immune Response in Cancer. *Cells*. MDPI AG. 2021;2245. Available from: <https://doi.org/10.3390/cells10092245>
- Balduzzi S, Rücker G, Schwarzer G. How to perform a meta-analysis with R: a practical tutorial. *Evid Based Mental Health*. BMJ. 2019;153–60. Available from: <https://doi.org/10.1136/ebmental-2019-300117>
- Baracco EE, Petrazzuolo A, Kroemer G. Assessment of annexin A1 release during immunogenic cell death. *Methods in Enzymology*. Elsevier 2019;71–9. Available from: <https://doi.org/10.1016/bs.mie.2019.06.010>
- Bindea G, Mlecnik B, Tosolini M, Kirilovsky A, Waldner M, Obenauf AC, et al. Spatiotemporal Dynamics of Intratumoral Immune Cells Reveal the Immune Landscape in Human Cancer. *Immunity*. Elsevier BV. 2013;782–95. Available from: <https://doi.org/10.1016/j.immuni.2013.10.003>
- Cao J, Zhang M, Zhang L, Lou J, Zhou F, Fang M. Non-coding RNA in thyroid cancer - Functions and mechanisms. *Cancer Letters*. Elsevier BV. 2021;117–26. Available from: <https://doi.org/10.1016/j.canlet.2020.08.021>
- Chen X, Zhang X, Qian Y, Xia E, Wang Y, Zhou Q. Ultrasound-targeted microbubble destruction-mediated miR-144–5p overexpression enhances the anti-tumor effect of paclitaxel on thyroid carcinoma by targeting STON2. *Cell Cycle*. Informa UK Limited. 2022a;1058–76. Available from: <https://doi.org/10.1080/15384101.2022.2040778>
- Chen Y, Zhu S, Liu T, Zhang S, Lu J, Fan W, et al. Epithelial cells activate fibroblasts to promote esophageal cancer development. *Cancer Cell*. Elsevier BV. 2023;903–918. e8. Available from: <https://doi.org/10.1016/j.ccell.2023.03.001>
- Chen Z, Wang Y, Li D, Le Y, Han Y, Jia L, et al. Single-Cell RNA Sequencing Revealed a 3-Gene Panel Predicted the Diagnosis and Prognosis of Thyroid Papillary Carcinoma and Associated With Tumor Immune Microenvironment. *Front. Oncol. Frontiers Media SA*. 2022b. Available from: <https://doi.org/10.3389/fonc.2022.862313>
- Chou R, Dana T, Haymart M, Leung AM, Tufano RP, Sosa JA, et al. Active Surveillance Versus Thyroid Surgery for Differentiated Thyroid Cancer: A Systematic Review. *Thyroid*. Mary Ann Liebert Inc. 2022;351–67. Available from: <https://doi.org/10.1089/thy.2021.0539>
- Efremova M, Vento-Tormo M, Teichmann SA, Vento-Tormo R. CellPhoneDB: inferring cell–cell communication from combined expression of multi-subunit ligand–receptor complexes. *Nat Protoc*. Springer Science and Business Media LLC. 2020;1484–506. Available from: <https://doi.org/10.1038/s41596-020-0292-x>
- Fallahi P, Ferrari SM, Galdiero MR, Varricchi G, Elia G, Ragusa F, et al. Molecular targets of tyrosine kinase inhibitors in thyroid cancer. *Seminars in Cancer Biology*. Elsevier BV. 2022;180–96. Available from: <https://doi.org/10.1016/j.semcancer.2020.11.013>
- Fang L, Che Y, Zhang C, Huang J, Lei Y, Lu Z, et al. LAMC1 upregulation via TGFβ induces inflammatory cancer-associated fibroblasts in esophageal squamous cell carcinoma via NF-κB–CXCL1–STAT3. *Molecular Oncology*. Wiley. 2021;3125–46. Available from: <https://doi.org/10.1002/1878-0261.13053>
- Fang Z, Tian Y, Sui C, Guo Y, Hu X, Lai Y, et al. Single-Cell Transcriptomics of Proliferative Phase Endometrium: Systems Analysis of Cell–Cell Communication Network Using CellChat. *Front Cell Dev Biol. Frontiers Media SA* 2022. Available from: <https://doi.org/10.3389/fcell.2022.919731>
- Feng J, Lu S-S, Xiao T, Huang W, Yi H, Zhu W, et al. ANXA1 Binds and Stabilizes EphA2 to Promote Nasopharyngeal Carcinoma Growth and Metastasis. *Cancer Research*. American Association for Cancer Research (AACR). 2020;4386–98. Available from: <https://doi.org/10.1158/0008-5472.can-20-0560>
- Feng Q, Ma X, Cheng K, Liu G, Li Y, Yue Y, et al. Engineered Bacterial Outer Membrane Vesicles as Controllable Two-Way Adaptors to Activate Macrophage Phagocytosis for Improved Tumor Immunotherapy. *Advanced Materials*. Wiley. 2022. Available from: <https://doi.org/10.1002/adma.202206200>
- Ferrari SM, Fallahi P, Galdiero MR, Ruffilli I, Elia G, Ragusa F, et al. Immune and Inflammatory Cells in Thyroid Cancer Microenvironment. *IJMS*. MDPI AG. 2019;4413. Available from: <https://doi.org/10.3390/ijms20184413>
- Foo SL, Yap G, Cui J, Lim LHK. Annexin-A1 – A Blessing or a Curse in Cancer?. *Trends in Molecular Medicine*. Elsevier BV. 2019;315–27. Available from: <https://doi.org/10.1016/j.molmed.2019.02.004>
- Franchini F, Palatucci G, Colao A, Ungaro P, Macchia PE, Nettore IC. Obesity and Thyroid Cancer Risk: An Update. *IJERPH*. MDPI AG. 2022;1116. Available from: <https://doi.org/10.3390/ijerph19031116>
- Fu C, Jiang A. Dendritic Cells and CD8 T Cell Immunity in Tumor Microenvironment. *Front Immunol Frontiers Media SA*. 2018. Available from: <https://doi.org/10.3389/fimmu.2018.03059>
- Garcia-Alvarez A, Hernando J, Carmona-Alonso A, Capdevila J. What is the status of immunotherapy in thyroid neoplasms?. *Front Endocrinol Frontiers Media SA*. 2022. Available from: <https://doi.org/10.3389/fendo.2022.929091>
- Garris CS, Luke JJ. Dendritic Cells, the T-cell-inflamed Tumor Microenvironment, and Immunotherapy Treatment Response. *Clinical Cancer Research*. American Association for Cancer Research (AACR); 2020. p. 3901–7. Available from: <https://doi.org/10.1158/1078-0432.ccr-19-1321>
- Gong P-J, Shao Y-C, Yang Y, Song W-J, He X, Zeng Y-F, et al. Analysis of N6-Methyladenosine Methyltransferase

- Reveals METTL14 and ZC3H13 as Tumor Suppressor Genes in Breast Cancer. *Front Oncol Frontiers Media SA*. 2020. Available from: <https://doi.org/10.3389/fonc.2020.578963>
- Grandclaoudon M, Perrot-Dockès M, Trichot C, Karpf L, Abouzid O, Chauvin C, et al. A Quantitative Multivariate Model of Human Dendritic Cell-T Helper Cell Communication. *Cell Elsevier BV*. 2019;432–447.e21. Available from: <https://doi.org/10.1016/j.cell.2019.09.012>
- Gulubova M, Ivanova K, Ananiev J, Gerenova J, Zdravski A, Stoyanov H, et al. VEGF expression, microvessel density and dendritic cell decrease in thyroid cancer. *Biotechnology & Biotechnological Equipment*. Informa UK Limited. 2014;508–17. Available from: <https://doi.org/10.1080/13102818.2014.909151>
- Guo H, Ha C, Dong H, Yang Z, Ma Y, Ding Y. Cancer-associated fibroblast-derived exosomal microRNA-98–5p promotes cisplatin resistance in ovarian cancer by targeting CDKN1A. *Cancer Cell Int*. Springer Science and Business Media LLC; 2019. Available from: <https://doi.org/10.1186/s12935-019-1051-3>
- Hänzelmann S, Castelo R, Guinney J. GSEA: gene set variation analysis for microarray and RNA-Seq data. *BMC Bioinformatics*. Springer Science and Business Media LLC; 2013. Available from: <https://doi.org/10.1186/1471-2105-14-7>
- Hao Y, Hao S, Andersen-Nissen E, Mauck WM III, Zheng S, Butler A, et al. Integrated analysis of multimodal single-cell data. *Cell Elsevier BV*; 2021;3573–3587.e29. Available from: <https://doi.org/10.1016/j.cell.2021.04.048>
- Hinshaw DC, Shevde LA. The Tumor Microenvironment Inately Modulates Cancer Progression. *Cancer Research*. American Association for Cancer Research (AACR). 2019;4557–66. Available from: <https://doi.org/10.1158/0008-5472.can-18-3962>
- Hou Y, Zhang Q, Pang W, Hou L, Liang Y, Han X, et al. YTHDC1-mediated augmentation of miR-30d in repressing pancreatic tumorigenesis via attenuation of RUNX1-induced transcriptional activation of Warburg effect. *Cell Death Differ*. Springer Science and Business Media LLC 2021;3105–24. Available from: <https://doi.org/10.1038/s41418-021-00804-0>
- Huang W-Y, Jheng L-C, Hsieh T-H, Ho K-S, Wang Y-Z, Gao Y-J, et al. Calcined Co(II)-Triethylenetetramine, Co(II)-Polyaniline-Thiourea as the Cathode Catalyst of Proton Exchanged Membrane Fuel Cell. *Polymers*. MDPI AG 2020;3070. Available from: <https://doi.org/10.3390/polym12123070>
- Jin L, Gu Y, Zhu Q, Li X, Jiang G. The role of ferroptosis-related genes for overall survival prediction in breast cancer. *Clinical Laboratory Analysis*. Wiley. 2021. Available from: <https://doi.org/10.1002/jcla.24094>
- Jin S, Plikus MV, Nie Q. CellChat for systematic analysis of cell–cell communication from single-cell transcriptomics. *Nat Protoc*. Springer Science and Business Media LLC. 2024;180–219. Available from: <https://doi.org/10.1038/s41596-024-01045-4>
- Kakudo K, Liu Z, Bai Y, Li Y, Kitayama N, Satoh S, et al. How to identify indolent thyroid tumors unlikely to recur and cause cancer death immediately after surgery—Risk stratification of papillary thyroid carcinoma in young patients—. *Endocr J*. Japan Endocrine Society 2021;871–80. Available from: <https://doi.org/10.1507/endocrj.ej21-0018>
- Le Naour J, Liu P, Zhao L, Adjemian S, Sztupinski Z, Taieb J, et al. A TLR3 Ligand Reestablishes Chemotherapeutic Responses in the Context of FPR1 Deficiency. *Cancer Discovery*. American Association for Cancer Research (AACR) 2021;408–23. Available from: <https://doi.org/10.1158/2159-8290.cd-20-0465>
- Li G, He J, Wang Q. Progress on cancer associated fibroblasts in tumor immunoregulation. *Zhejiang Da Xue Xue Bao Yi Xue Ban*. China 2018;47(5):558–63.
- Li P-H, Kong X-Y, He Y-Z, Liu Y, Peng X, Li Z-H, et al. Recent developments in application of single-cell RNA sequencing in the tumour immune microenvironment and cancer therapy. *Military Med Res*. Springer Science and Business Media LLC. 2022a. Available from: <https://doi.org/10.1186/s40779-022-00414-y>
- Li Z, Lai X, Fu S, Ren L, Cai H, Zhang H, et al. Immunogenic Cell Death Activates the Tumor Immune Microenvironment to Boost the Immunotherapy Efficiency. *Advanced Science*. Wiley. 2022b. Available from: <https://doi.org/10.1002/advs.202201734>
- Liu S. MiR-374a/b-5p Suppresses Cell Growth in Papillary Thyroid Carcinoma Through Blocking Exosomal ANXA1-Induced Macrophage M2 Polarization. *Biochem Genet*. Springer Science and Business Media LLC. 2024;1258–74. Available from: <https://doi.org/10.1007/s10528-024-10747-z>
- Luo L, Xia L, Zha B, Zuo C, Deng D, Chen M, et al. miR-335–5p targeting ICAM-1 inhibits invasion and metastasis of thyroid cancer cells. *Biomedicine & Pharmacotherapy*. Elsevier BV 2018;983–90. Available from: <https://doi.org/10.1016/j.biopha.2018.07.046>
- Luo W, Hoang H, Liao Y, Pan J, Ayello J, Cairo MS. A humanized orthotopic mouse model for preclinical evaluation of immunotherapy in Ewing sarcoma. *Front Immunol*. Frontiers Media SA. 2023. Available from: <https://doi.org/10.3389/fimmu.2023.1277987>
- Meng Y, Zhao Q, An L, Jiao S, Li R, Sang Y, et al. A TNFR2–hnRNPK Axis Promotes Primary Liver Cancer Development via Activation of YAP Signaling in Hepatic Progenitor Cells. *Cancer Research*. American Association for Cancer Research (AACR) 2021;3036–50. Available from: <https://doi.org/10.1158/0008-5472.can-20-3175>
- Min Y, Han D, Fu Z, Wang H, Liu L, Tian Y. &alpha;-MSH inhibits TNF-&alpha;-induced maturation of human dendritic cells *in vitro* through the up-regulation of ANXA1. *ABBS*. China Science Publishing & Media Ltd. 2011;61–8. Available from: <https://doi.org/10.1093/abbs/gmq109>
- Mokuda S, Miyazaki T, Ubara Y, Kanno M, Sugiyama E, Takasugi K, et al. CD1a+ survivin+ dendritic cell infiltration in dermal lesions of systemic sclerosis. *Arthritis Res Ther*. Springer Science and Business Media LLC 2015. Available from: <https://doi.org/10.1186/s13075-015-0785-0>
- Muir CA, Tsang VHM, Menzies AM, Clifton-Bligh RJ. Immune Related Adverse Events of the Thyroid – A Narrative Review. *Front Endocrinol*. Frontiers Media SA

2022. Available from: <https://doi.org/10.3389/fendo.2022.886930>
- Pansy K, Uhl B, Krstic J, Szmyra M, Fechter K, Santiso A, et al. Immune Regulatory Processes of the Tumor Microenvironment under Malignant Conditions. *IJMS*. MDPI AG 2021;13311. Available from: <https://doi.org/10.3390/ijms222413311>
- Peng X, He Y, Huang J, Tao Y, Liu S. Metabolism of Dendritic Cells in Tumor Microenvironment: For Immunotherapy. *Front. Immunol. Frontiers Media SA* 2021. Available from: <https://doi.org/10.3389/fimmu.2021.613492>
- Portella L, Bello AM, Scala S. CXCL12 Signaling in the Tumor Microenvironment. *Advances in Experimental Medicine and Biology*. Cham: Springer International Publishing 2021;51–70. Available from: [https://doi.org/10.1007/978-3-030-62658-7\\_5](https://doi.org/10.1007/978-3-030-62658-7_5)
- Prete A, Borges de Souza P, Censi S, Muzza M, Nucci N, Sponziello M. Update on Fundamental Mechanisms of Thyroid Cancer. *Front. Endocrinol. Frontiers Media SA* 2020. Available from: <https://doi.org/10.3389/fendo.2020.00102>
- Qiu X, Mao Q, Tang Y, Wang L, Chawla R, Pliner HA, et al. Reversed graph embedding resolves complex single-cell trajectories. *Nat Methods*. Springer Science and Business Media LLC 2017;979–82. Available from: <https://doi.org/10.1038/nmeth.4402>
- Ritchie ME, Phipson B, Wu D, Hu Y, Law CW, Shi W, et al. limma powers differential expression analyses for RNA-seq and microarray studies. *Nucleic Acids Research*. Oxford University Press (OUP) 2015;e47–e47. Available from: <https://doi.org/10.1093/nar/gkv007>
- Ronca V, Wootton G, Milani C, Cain O. The Immunological Basis of Liver Allograft Rejection. *Front. Immunol. Frontiers Media SA* 2020. Available from: <https://doi.org/10.3389/fimmu.2020.02155>
- Sellars MC, Wu CJ, Fritsch EF. Cancer vaccines: Building a bridge over troubled waters. *Cell Elsevier BV* 2022;2770–88. Available from: <https://doi.org/10.1016/j.cell.2022.06.035>
- Senchenkova EY, Ansari J, Becker F, Vital SA, Al-Yafeai Z, Sparkenbaugh EM, et al. Novel Role for the AnxA1-Fpr2/ALX Signaling Axis as a Key Regulator of Platelet Function to Promote Resolution of Inflammation. *Circulation Ovid Technologies (Wolters Kluwer Health)* 2019;319–35. Available from: <https://doi.org/10.1161/circulationaha.118.039345>
- Tauriello DVF, Sancho E, Battle E. Overcoming TGFβ-mediated immune evasion in cancer. *Nat Rev Cancer*. Springer Science and Business Media LLC 2021;25–44. Available from: <https://doi.org/10.1038/s41568-021-00413-6>
- Tian Z, Zhang P, Li X, Jiang D. Analysis of immunogenic cell death in ascending thoracic aortic aneurysms based on single-cell sequencing data. *Front Immunol Frontiers Media SA* 2023. Available from: <https://doi.org/10.3389/fimmu.2023.1087978>
- Tong Y, Huang J, Ren W, Yu J, Zhang X, Wang Z, et al. Association of tumor immune microenvironment profiling and 21-gene recurrence assay in early breast cancer patients. *Eur J Med Res Springer Science and Business Media LLC* 2022. Available from: <https://doi.org/10.1186/s40001-022-00917-3>
- Ulisse S, Baldini E, Lauro A, Pironi D, Tripodi D, Lori E, et al. Papillary Thyroid Cancer Prognosis: An Evolving Field. *Cancers*. MDPI AG 2021;5567. Available from: <https://doi.org/10.3390/cancers13215567>
- Vecchi L, Alves Pereira Zóia M, Goss Santos T, de Oliveira Beserra A, Colaço Ramos CM, França Matias Colombo B, et al. Inhibition of the AnxA1/FPR1 autocrine axis reduces MDA-MB-231 breast cancer cell growth and aggressiveness in vitro and in vivo. *Biochimica et Biophysica Acta (BBA) - Molecular Cell Research*. Elsevier BV 2018;1368–82. Available from: <https://doi.org/10.1016/j.bbamcr.2018.06.010>
- Vecchi L, Mota STS, Zóia MAP, Martins IC, de Souza JB, Santos TG, et al. Interleukin-6 Signaling in Triple Negative Breast Cancer Cells Elicits the Annexin A1/Formyl Peptide Receptor 1 Axis and Affects the Tumor Microenvironment. *Cells*. MDPI AG 2022;1705. Available from: <https://doi.org/10.3390/cells11101705>
- Wang K, Jiang L, Zhang Y, Chen C. <p>Progression of Thyroid Carcinoma Is Promoted by the m6A Methyltransferase METTL3 Through Regulating m6A Methylation on TCF1</p>. *OTT*. Informa UK Limited 2020a;1605–12. Available from: <https://doi.org/10.2147/ott.s234751>
- Wang M, Liu J, Zhao Y, He R, Xu X, Guo X, et al. Upregulation of METTL14 mediates the elevation of PERP mRNA N6 adenosine methylation promoting the growth and metastasis of pancreatic cancer. *Mol Cancer*. Springer Science and Business Media LLC. 2020b. Available from: <https://doi.org/10.1186/s12943-020-01249-8>
- Wang Y, Li Y, Zhong J, Li M, Zhou Y, Lin Q, et al. Tumor-derived Cav-1 promotes pre-metastatic niche formation and lung metastasis in breast cancer. *Theranostics*. Ivyspring International Publisher 2023;1684–97. Available from: <https://doi.org/10.7150/thno.79250>
- Wang Y, Xiang Y, Xin VW, Wang X-W, Peng X-C, Liu X-Q, et al. Dendritic cell biology and its role in tumor immunotherapy. *J Hematol Oncol*. Springer Science and Business Media LLC. 2020c. Available from: <https://doi.org/10.1186/s13045-020-00939-6>
- Wang Z, Gerstein M, Snyder M. RNA-Seq: a revolutionary tool for transcriptomics. *Nat Rev Genet*. Springer Science and Business Media LLC. 2009;57–63. Available from: <https://doi.org/10.1038/nrg2484>
- Wculek SK, Cueto FJ, Mujal AM, Melero I, Krummel MF, Sancho D. Dendritic cells in cancer immunology and immunotherapy. *Nat Rev Immunol*. Springer Science and Business Media LLC. 2019;7–24. Available from: <https://doi.org/10.1038/s41577-019-0210-z>
- Wu L, Wu W, Zhang J, Zhao Z, Li L, Zhu M, et al. Natural Coevolution of Tumor and Immunoenvironment in Glioblastoma. *Cancer Discovery*. American Association for Cancer Research (AACR) 2022;2820–37. Available from: <https://doi.org/10.1158/2159-8290.cd-22-0196>
- Xiao D, Zeng T, Zhu W, Yu Z-Z, Huang W, Yi H, et al. ANXA1 Promotes Tumor Immune Evasion by Binding PARP1 and Upregulating Stat3-Induced Expression of PD-L1 in Multiple Cancers. *Cancer Immunology Research*. American Association for Cancer Research

- (AACR) 2023;1367–83. Available from: <https://doi.org/10.1158/2326-6066.cir-22-0896>
- Xie Z, Li X, He Y, Wu S, Wang S, Sun J, et al. Immune Cell Confrontation in the Papillary Thyroid Carcinoma Microenvironment. *Front Endocrinol. Frontiers Media SA*. 2020. Available from: <https://doi.org/10.3389/fendo.2020.570604>
- Xu Y, Lin S, Tao J, Liu X, Zhou R, Chen S, et al. Correlation research of susceptibility single nucleotide polymorphisms and the severity of clinical symptoms in attention deficit hyperactivity disorder. *Front Psychiatry Frontiers Media SA*. 2022. Available from: <https://doi.org/10.3389/fpsy.2022.1003542>
- Yu G, Wang L-G, Han Y, He Q-Y. clusterProfiler: an R Package for Comparing Biological Themes Among Gene Clusters. *OMICS: A Journal of Integrative Biology. Mary Ann Liebert Inc* 2012;284–7. Available from: <https://doi.org/10.1089/omi.2011.0118>
- Zanfardino M, Pane K, Mirabelli P, Salvatore M, Franzese M. TCGA-TCIA Impact on Radiogenomics Cancer Research: A Systematic Review. *IJMS. MDPI AG* 2019;6033. Available from: <https://doi.org/10.3390/ijms20236033>
- Zhang Q, Tang Y, Hu G, Yuan Z, Zhang S, Sun Y, et al. Comprehensive pan-cancer analysis identifies cellular senescence as a new therapeutic target for cancer: multi-omics analysis and single-cell sequencing validation. *Am J Cancer Res. United States* 2022;12(9):4103–19.
- Zhao J, Guo C, Ma Z, Liu H, Yang C, Li S. Identification of a novel gene expression signature associated with overall survival in patients with lung adenocarcinoma: A comprehensive analysis based on TCGA and GEO databases. *Lung Cancer. Elsevier BV* 2020;90–6. Available from: <https://doi.org/10.1016/j.lungcan.2020.09.014>
- Zhao L, Wang W, Niu P, Luan X, Zhao D, Chen Y. The molecular mechanisms of CTHRC1 in gastric cancer by integrating TCGA, GEO and GSA datasets. *Front Genet Frontiers Media SA*. 2022. Available from: <https://doi.org/10.3389/fgene.2022.900124>
- Zhao W, Liu M, Zhang M, Wang Y, Zhang Y, Wang S, et al. Effects of Inflammation on the Immune Microenvironment in Gastric Cancer. *Front. Oncol. Frontiers Media SA*. 2021. Available from: <https://doi.org/10.3389/fonc.2021.690298>
- Zheng T, Zhou Y, Xu X, Qi X, Liu J, Pu Y, et al. MiR-30c-5p loss-induced PELI1 accumulation regulates cell proliferation and migration via activating PI3K/AKT pathway in papillary thyroid carcinoma. *J Transl Med Springer Science and Business Media LLC*. 2022. Available from: <https://doi.org/10.1186/s12967-021-03226-1>
- Zhou X, Yang J, Lu Y, Ma Y, Meng Y, Li Q, et al. Relationships of tumor differentiation and immune infiltration in gastric cancers revealed by single-cell RNA-seq analyses. *Cell Mol Life Sci. Springer Science and Business Media LLC*. 2023. Available from: <https://doi.org/10.1007/s00018-023-04702-1>
- Zhuang Y, Wang L, Guo J, Sun D, Wang Y, Liu W, et al. Molecular recognition of formylpeptides and diverse agonists by the formylpeptide receptors FPR1 and FPR2. *Nat Commun. Springer Science and Business Media LLC*. 2022. Available from: <https://doi.org/10.1038/s41467-022-28586-0>

**Publisher's Note** Springer Nature remains neutral with regard to jurisdictional claims in published maps and institutional affiliations.